
Sea-ice in decadal and long-term simulations with the Max Planck Institute Earth System Model

Melanie Bräu



Munich 2013

Meereis in dekadischen und Langzeitsimulationen mit dem Max Planck Institute Earth System Model

Melanie Bräu



München 2013

Ludwig-Maximilians-Universität München
Faculty of Physics
Meteorological Institute Munich

**Sea-ice in decadal and long-term simulations
with the Max Planck Institute Earth System
Model**

Melanie Bräu

BACHELOR THESIS

Supervisor: Priv.-Doz. Dr. habil. Veronika Eyring (DLR)

Deutsches Zentrum für Luft- und Raumfahrt (DLR)
Institut für Physik der Atmosphäre

July 2013

Abstract

A new type of simulations, so-called decadal predictions, was part of the Coupled Model Intercomparison Project Phase 5 (CMIP5) protocol. In contrast to long-term simulations that are run by global Earth system models (ESMs) to project future climate under various forcing scenarios, the decadal short-term (~10-30 years) simulations aim at predicting some aspects of slow natural variability by initializing the simulations from an observed climate state. In this work, the representation of sea-ice in the CMIP5 initialized decadal predictions from the Max Planck Institute Earth System Model (MPI-ESM) is compared to the one from the MPI-ESM uninitialized free-running hindcast simulations from this model and to observations. The aim of the work is to start exploring the science question whether the initial conditions in the hindcast lead to more accurate retrospective predictions of sea-ice compared to the uninitialized simulations. Each ensemble member of the MPI-ESM decadal simulations is initialized with a standalone experiment from the underlying ocean model (MPI-OM) at the end of the previous year. In this simulation temperature and salinity anomalies are nudged towards three-dimensional ocean fields from the National Center of Environmental Predictions (NCEP) / National Oceanic and Atmospheric Administration (NOAA) reanalysis. For the evaluation, the observational datasets of the Advanced Microwave Scanning Radiometer-Earth observing System (AMSR-E), the National Snow and Ice Data Center (NSIDC) and the Hadley Centre Sea Ice and Sea Surface Temperature (HadISST) were used.

As has been found in previous studies, the CMIP5 models and observations display a negative trend of September mean Arctic sea-ice extent from 1960-2005 with a large spread among the individual climate models both in terms of absolute values and in terms of trends. September mean Arctic sea-ice extent is well represented by both the uninitialized and initialized MPI-ESM simulations. The qualitative comparison of the two sets of simulations that is presented in this work shows no substantial differences in the simulation of trends, the annual cycle and spatial distribution September Arctic sea-ice extent. Follow-up studies should build up a verification system to further study the question of Arctic sea-ice predictability before a final answer can be given. March mean Antarctic sea-ice extent in most of the CMIP5 long-term uninitialized simulations has a small trend over the time period 1960-2005 in agreement with observations, but the majority of the models is biased low. The low bias is also present in the MPI-ESM in both the uninitialized and the initialized simulations. Again no significant differences can be found in the qualitative analysis applied in this work and further studies are needed to assess predictability.

Content

| | |
|--|----|
| 1 Introduction | 11 |
| 1.1 Background and Motivation..... | 11 |
| 1.2 Structure of the Thesis..... | 12 |
| 2 Scientific Background..... | 12 |
| 2.1 Sea-Ice..... | 12 |
| 2.2 Near-term Experiments (Decadal Predictions) | 13 |
| 3 Model, Model Simulations and Evaluation Concept..... | 15 |
| 3.1 Max Planck Institute Earth System Model (MPI-ESM)..... | 15 |
| 3.1.1 Overview..... | 15 |
| 3.1.2 MPI-ESM Sea-ice Module..... | 16 |
| 3.2 Model Simulations with the MPI-ESM..... | 18 |
| 3.2.1 CMIP5 Protocol for Decadal Simulations..... | 18 |
| 3.2.2 MPI-ESM Simulations..... | 19 |
| 3.3 Evaluation and Verification Concept..... | 21 |
| 3.3.1 Qualitative evaluation..... | 21 |
| 3.3.2 Outlook Quantitative Evaluation for Follow-up Studies..... | 21 |
| 4 Results..... | 22 |
| 4.1 Arctic Sea-ice..... | 22 |
| 4.2 Antarctic Sea-ice..... | 31 |
| 5 Summary and Outlook..... | 39 |
| 6 Acknowledgements..... | 40 |
| 7 References..... | 41 |

1 Introduction

1.1 Background and Motivation

Even though sea-ice is just a thin layer that represents the boundary between two much larger geophysical fluids, the ocean and the atmosphere, it has strong impact on oceanic and atmospheric circulations and the planetary heat budget. In the last few decades sea-ice cover in the Arctic has declined on a large scale. In all the years from 2007-2012 the sea-ice extent in summer reached a minimum since the beginning of satellite observation in 1978 [Richter-Menge et al., 2012]. The decline of September mean sea-ice extent was observed to be -12.9 ± 1.47 % per decade in the years 1978-2011 which leads to an overall sea-ice decline of more than 30% for this time period [Stroeve et al., 2012].

A different development is recorded for the Antarctic. The September minimum sea-ice extent balances around the same state. The Antarctic sea-ice extent in March shows high variability with an observed small trend of -1.7 ± -2.3 %/decade over the period 1973-2006. Reasons for the small observed sea-ice extent trend over Antarctica that are discussed in the literature are for example that the katabatic winds remove surface heat from the surface so that the underlying sea-ice is not influenced. This wind also creates a near-surface cold-water layer with coastal water. Since the Antarctic is surrounded just by water, it is isolated to warmer regions due to wind systems and oceanic streams [Stroeve et al., 2007].

Globally model simulations show a continuing rise in global mean surface temperature and project a further increase in the 21st century with rising greenhouse gas concentrations [IPCC,2007]. The global climate is influenced by external forcing factors but also by natural variability occurring on shorter time-scales [Smith et al., 2012]. Many different stakeholders such as natural resource industries, fishing communities, commercial shippers, marine tourism operators, local populations and the scientific research community show interest in the near-term evolution of climate and, related to this work, changes in Arctic sea-ice [Richter-Menge et al., 2012].

Therefore, a new set of near-term simulations (10-30 years) called decadal predictions initialized from observed climate states has been run by multiple models as part of the 5th phase of the Coupled Model Intercomparison Project (CMIP5) [Taylor et al., 2012] in support of the Intergovernmental Panel in Climate Change (IPCC) Fifth Assessment Report (AR5). A benefit from initialization is to begin the simulation at the observed climate state to capture not only the impact of changing composition but also the evolution of slow natural variability [Solomon et al., 2010]. In addition, these models performed the uninitialized long-term simulations from 1850 to 2005. Previous studies indicate some skill from decadal simulations matching observed variability [e.g., Goddard et al., 2012, Smith et al., 2012].

Decadal prediction experiments are a new area of research and the set-up and skill of these simulations still has to be tested. The verification of hindcasts is essential for predictions to improve errors in initialization strategies, model initialization of natural variability and model responses to external forcing. Additional uncertainties for predictions come from future external forcing factors [Smith et al., 2012].

The goal of this work is to qualitatively compare the representation of sea-ice in the initialized decadal prediction hindcasts of the Max-Planck-Institute – Earth System Model (MPI-ESM) to the

uninitialized free-running long-term hindcasts from this model and to observations. In addition, the uninitialized hindcast simulations of the MPI-ESM are set in the context of other CMIP5 climate models by comparing the minimum sea-ice extent of the Arctic and Antarctic for the historical period 1960-2005. For the analysis of the decadal simulations, both the decadal hindcast (1960-2005) and the prediction experiments (2006-2020) are included to provide a time-range from 1960-2020. The experiments beyond 2005 are forced with the Representative Concentration Pathway (RCP) 4.5. The emphasis of this work is on a single 10 year hindcast simulation with a set of ten ensemble members starting in 1996 in order to start exploring the science question: do the initial conditions in the hindcast lead to more accurate retrospective predictions of sea-ice compared to the uninitialized simulations and if so, on what time scales?

This work follows on from Hübner (2013) and Notz et al. (2013) who evaluated the representation of sea-ice in the uninitialized MPI-ESM simulations.

1.2 Structure of the Thesis

This thesis contains five chapters. Chapter 2 briefly presents the scientific background for sea-ice and the decadal predictions. Chapter 3 provides brief information about the Earth System Model MPI-ESM and its components and the simulations of the model used and evaluated in this work. The results are presented in Chapter 4 for the Arctic (Section 4.1) and the Antarctic (Section 4.2). Chapter 5 summarizes this work and gives an outlook.

2 Scientific Background

2.1 Sea-Ice

Sea-ice is frozen ocean water that occurs in the Arctic and Antarctic. It has an annual cycle reaching a maximum of area and thickness in the winter months and a minimum in summer. In some regions sea ice remains all year long (NSIDC, 11.07.2013). Despite its limited areal expansion and the fact that sea ice is just a thin layer between the ocean and the atmosphere, sea ice influences the global climate and reacts very sensitive to climate change. It is therefore an important indicator for testing the sensitivity of models to climate change [Notz et al., 2013].

Not only the decline in sea-ice extent, thickness and the extension of the summer melting season, also the formation from multiyear to seasonal ice is striking. In September 2011 for example only 25% of the sea-ice was older than two years in comparison to the 1980s when there were 50-60% [Stroeve et al., 2012]. At the begin of the melting season the albedo of seasonal sea-ice drops from around 0.85 for snow and can reach a minimum at 0.2. Therefore the reflectivity is less and the total amount of heat input on sea ice increases. As a result more sea-ice is melting in the summer period and the transmission of sunlight to the ocean enforced. This in turn will rise the temperature in the upper ocean and finally lead to more sea-ice melting. The described loop is an example for a positive climate feedback and the reason for the high sensitivity to climate change [Perovich, Polashensski, 2012].

There are different measures to quantify the formation of sea-ice. The sea-ice concentration is a unit-less measure. A 100% sea ice concentration stands for a completely ice covered grid cell, 0% respectively for no sea-ice [NSIDC, 11.07.2013]. The measure mostly used in this work is the sea ice extent which is the sum of the area of all grid cells that are covered by at least 15% sea-ice concentration [Stroeve et al., 2007]. The sea ice extent is therefore greater than the actual sea ice area and is typically specified in square kilometers. The extent has advantages in minimizing model noise and enabling comparisons between different models and observations [NSIDC, 11.07.2013].

2.2 Near-term Experiments (Decadal Predictions)

Climate in the near-term future is not only influenced by external forcing factors like changes in greenhouse gases, anthropogenic aerosols, volcanic aerosols and solar irradiance. Natural internal variability plays a non-negligible role. Near-term decadal simulations (~10-30 years) are initialized from the observed system. They therefore start from the correct phase of the system with the goal to predict some aspects of natural variability. Examples of recurrent natural events initiating natural variability are the El Niño Southern Oscillation (ENSO), the North Atlantic Oscillation (NAO) or the Madden-Julian Oscillation (MJO) [Smith et al., 2012]. Also events on less regular timescales like a record cold December belong to this category [Taylor et al., 2012].

Decadal climate simulations are initialized by observation data and run for a time period of about ten to thirty years with multiple ensemble members [Meehl et al., 2013]. The CMIP5 protocol recommended a minimum of three ensemble members for 10-yr hindcasts initialized from observed climate states near the years 1960, 1965, and every 5 years to 2005. Additionally it was recommended to extend these 10-yr hindcasts with an additional 20 year simulation, resulting into two 30-year hindcasts and one 30-year prediction to the year 2035 [Taylor et al., 2012]. The benefit of this technique is receiving less unpredictable noise and reducing observational uncertainty through initialization [Goddard et al., 2012]. The ensemble members are either taken from one model or from multiple models to form a multi-model ensemble.

Each ensemble member from a single model follows a specified nomenclature introduced by CMIP. The format used is “r<N>i<M>p<L>”. “N” stands for equally realistic outcomes for simulations that were started with different initial conditions (i.e., ensemble members). “M” indicates different initialization methods and “L” describes variations of perturbed model versions. “N”, “M” and “L” are all integers and it is recommended to assign sequentially beginning with 1 [Taylor et al., 2010].

Simulations on this timescale are divided into two categories: hindcasts and predictions. Decadal climate predictions show future development in regional climate statistics. In contrast, the term hindcast refers to predictions of past cases by climate models, which were initialized with observations for the same start periods [Meehl et al., 2013].

Examining climate prediction on decadal time scales is a very new attempt and is meant to fill the gap between interannual to decadal time scales and century-long climate projections [Pohlmann et al., 2009; Meehl et al., 2009; 2013]. Those long-term projections from climate models are started from a random point of preindustrial climate around 1850, free running and uninitialized [Smith et al., 2012]. The intention for these simulations is to project climate under varying external forcings [Taylor et al., 2012].

On the contrary decadal prediction experiments also called near-term experiments attempt to reproduce natural low-frequency climate variability as well as climate change through external

forcing [Goddard et al., 2012; Smith et al., 2012]. The state of initialization should therefore well represent the climate state of the start date [Pohlmann et al., 2009].

Due to initialization a bias might emerge, when the equilibrium state of the model does not exactly match the real equilibrium state [Meehl et al., 2013]. This bias is dependent on the utilized initialization method namely full field or anomaly initialization:

- Full field initialization implies that initial conditions are created by constraining model values to observed analysis. The drift from the initial state to the models preferred equilibrium state can be calculated from the uninitialized hindcast experiments and be subtracted from the model output [e.g., Meehl et al., 2009; Goddard et al., 2012].
- For the method anomaly initialization, observed anomalies are added to the model climatology [e.g., Meehl et al., 2009; Goddard et al., 2012].

The problem concerning these two methods is the following: climate models have each their preferred equilibrium they tend to drift, which coincides not in a perfect way with the real climate state. Once they are initialized by observations, models are forced to match observations. Processing the model run the model will tend to drift back to its preferred state [Taylor et al., 2012]. Figure 1 indicates schematically the bias drift through initialization once a misrepresentation between uninitialized model and observation trend exists (from Meehl et al., 2013). The points of initialization are displayed as colored dots color-coded for different start dates. The short term drift from initialization states to the models preferred states is represented with colored lines respectively. Compared to observations (black solid line) these equilibrium states (grey solid line) have a long-background trend which comes from imperfect modeling. The bias influences almost all variables on the decadal timescale [Taylor et al., 2012] and needs to be accounted for when calculating quantitative skill measures.

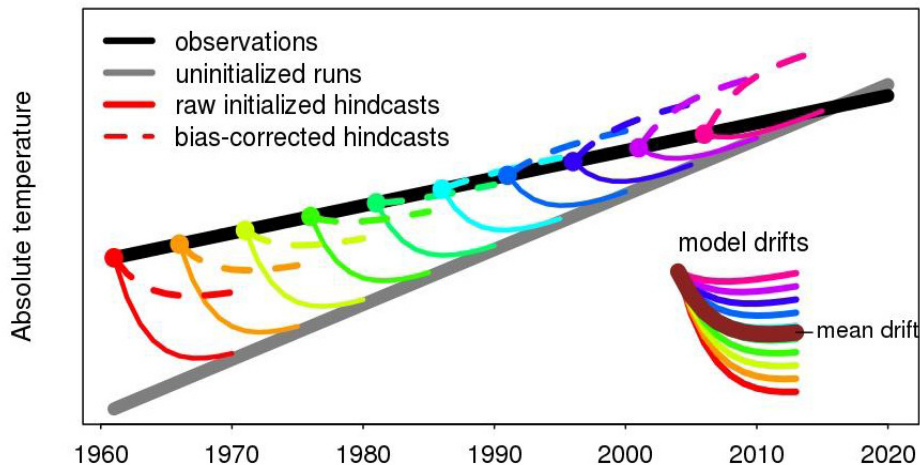


Figure 1: Bias adjustment for decadal hindcasts. The offset between the observation (black solid line) and the uninitialized simulation (grey solid line) leads to time depending drifts (colored solid lines) from the initialization (colored dots) to the models preferred state. Each color stands for a different initialization time. Bias adjustment is represented with colored dashed lines.

3 Model, Model Simulations and Evaluation Concept

This thesis evaluates the model simulations of the Max Planck Institute Earth System Model (MPI-ESM). Section 3.1 gives a brief overview of the MPI-ESM and Section 3.2 on the MPI-ESM sea-ice model. Section 3.3 describes model simulations for CMIP5 in general and as they are reassembled in this work.

3.1 Max Planck Institute Earth System Model (MPI-ESM)

3.1.1 Overview

The MPI-ESM is a further development of the ECHAM5/MPIOM coupled climate model of the Max-Planck-Institute for Meteorology (MPI-M) in Hamburg, Germany. The model embraces processes of the atmosphere, ocean and land surface through the exchange of energy, momentum, water and important tracer gases like carbon dioxide. It contains four model components namely the European Center-Hamburg atmosphere model (ECHAM6) [Stevens et al., 2012], the Max Planck Institute ocean model (MPIOM) [Jungclaus et al., 2012], Jena Scheme for Biosphere Atmosphere coupling in Hamburg (JSBACH) [Reick et al., 2012] simulating land-surface processes and Hamburg ocean Carbon Cycle Model (HAMOCC5) the biogeochemistry [Ilyina et al., 2012]. The coupling interface Ocean Atmosphere Sea Ice Soil (OASIS3) enables the coupling between atmosphere and land surface as well as ocean and biogeochemistry. Figure 2 provides a schematic overview of the components of the MPI-ESM (from [Giorgetta et al., 2013]).

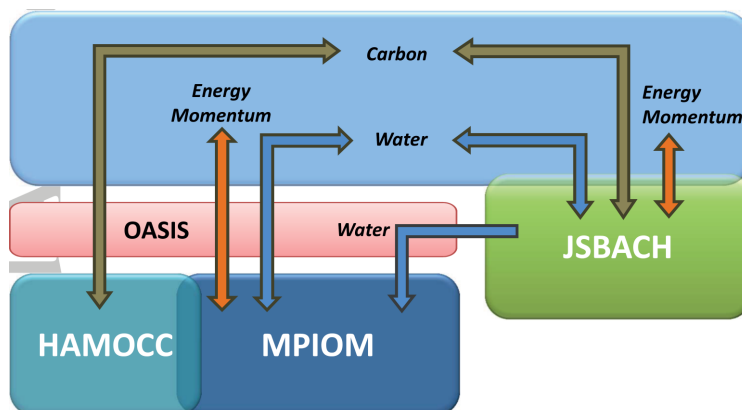


Figure 2: Scheme of the modules contained in the MPI-ESM. The blue box on top represents the atmosphere model ECHAM, the other boxes shaded in blue and green the models HAMOCC, MPIOM and JSBACH. OASIS3 is pictured in pink with arrows indicating the exchange of momentum and energy (orange), trace gases (brown) and water (blue).

One improvement of the MPI-ESM compared to the predecessor ECHAM5/MPIOM [Jungclaus et al., 2006] used for CMIP3 is the inclusion of a coupled carbon cycle to account for carbon cycle feedbacks. The carbon cycle is simulated by the HAMOCC5 (ocean) and the JSBACH (land) modules. Once a climate model contains a interactive carbon cycle and biogeochemical modules it is commonly referred to as Earth System model (ESM).

Changes have been made from ECHAM version 5 to 6 concerning the shortwave radiative transfer, representation of the middle atmosphere due to higher resolution and the calculations on surface albedo. In ECHAM5 the ocean surface albedo was regarded constant and is now containing the dependency on the zenith angle. For sea-ice and snow, melt ponds and the aging of snow are also included [Jungclaus et al. 2012], see also Section 3.2. To investigate various phenomena occurring on different scales, users have the opportunity to choose between higher and lower resolutions. Furthermore the representation of the land surface is improved by including the climate-consistent development of the geographic distribution of vegetation [Giorgetta et al., 2013].

The MPI-ESM has been implemented for CMIP5 at two resolutions: the MPI-ESM-LR is the low-resolution version with a bipolar grid, horizontal resolution of 1.5° and 40 vertical levels for the ocean. The two poles are located in the Antarctic and in Greenland. The mixed-resolution model MPI-ESM-MR has the same vertical resolution for the ocean, but contains three poles in Canada, Siberia and the Antarctic with a horizontal resolution of 0.4°. The horizontal resolution in the atmosphere is 1.9° with 47 vertical levels for the MPI-ESM-LR, whereas for the MPI-ESM-MR the vertical resolution of the atmosphere has 95 levels with a horizontal resolution of 1.9°. Comparing these two model versions, the MPI-ESM-MR offers higher resolution in most of the regions of the ocean except around Greenland and Antarctica [Notz et al, 2013].

3.1.2 MPI-ESM Sea-ice Module

Sea-ice is represented in the models for the atmosphere (ECHAM6) and the ocean (MPIOM). The model MPIOM contains a complete sea-ice submodel with little changes adopted from the predecessor ECHAM5/MPIOM [Notz et al., 2013]. The sea-ice module from the MPIOM consists of a dynamic and thermodynamic part. The motion of sea-ice in the dynamical part is described by the following two-dimensional momentum balance equation.

$$\frac{d}{dt} \vec{v}_i + f(\vec{k} \times \vec{v}_i) = -g \vec{\nabla} \zeta + \frac{\vec{\tau}_a}{\rho_i h_i} + \frac{\vec{\tau}_o}{\rho_i h_i} + \vec{\nabla} \sigma_{mn}$$

\vec{v}_i is the velocity vector of sea-ice, f the Coriolis parameter, \vec{k} the unit vector normal to the earth center, g the acceleration due to gravity and ζ the sea surface elevation, which can be derived from kinematic boundary conditions and incompressible conditions. The tensors $\vec{\tau}_a$ and $\vec{\tau}_o$ represent wind stress and ocean current stress, respectively and are divided by the product of the sea-ice density ρ_i and thickness h_i . The two-dimensional internal stress tensor σ_{mn} has the unit N/m² and describes the sea-ice rheology representing the sea-ice dynamics [Hibler, 1979]. The internal sea-ice stress can be expressed by the equation for a nonlinear viscous compressible fluid.

$$\sigma_{mn} = 2 \eta \epsilon_{mn} + [(\xi - \eta)(\epsilon_{11} + \epsilon_{22}) - \frac{P_i}{2}] \delta_{mn}$$

η and ξ are the shear and bulk viscosities depending on internal pressure and the ratio of the axes of the yield ellipse. This ellipse differs between internal linear-viscous and plastic boundary points [Marstrand et al., 2003], because sea-ice has plastic characteristics under stress conditions, but is regarded viscous when stress rates are small [Hunke E., Dukowicz J. , 1997]. ϵ_{mm} is the strain rate tensor and P_i the internal sea-ice pressure, which is a function of sea-ice thickness and subgrid-scale areal fractional sea-ice compactness. δ_{mm} is the Kronecker delta [Marstrand et al., 2003].

The thermodynamical part of the sea-ice submodel implicates local melt rates at the base of sea-ice and at the surface. The following equation describes the interface between the atmosphere and sea-ice/snow layer.

$$Q_a = (1 - I)Q_w + IQ_i$$

The net atmospheric heat flux Q_a is divided into the open water heat flux Q_w and the heat flux over sea-ice Q_i in terms of the fraction covered by sea-ice I using a subgrid-scale. The model includes the zero-layer formulation [Semtner, 1976] for sea-ice, which describes conductive heat flux Q_{cond} in the thermal equilibrium

$$Q_i + Q_{cond} = 0$$

with the following proportional relation:

$$Q_{cond} = k_i \frac{T_{freeze} - T_{surf}}{\tilde{h}_i}$$

T_{freeze} is the freezing temperature of sea water, T_{surf} the sea-ice/snow layer surface temperature and k_i the thermal conductivity. \tilde{h}_i describes the effective thermodynamic thickness of the sea-ice/snow layer, which comprises differences in thermal conductivity between snow and sea-ice. The significant difference in conductivity between snow and ice results in a seven times more effective isolation by snow. Thus just a thin layer of snow antagonizes heat loss to the atmosphere and leads to increased sea-ice thickness.

Once the sea-ice/snow surface temperature reaches more than 0°C, it is assumed that the remaining energy will melt the snow and then sea-ice. If the total sea-ice/snow cover is melted, the remaining energy is added to the open water heat flux. The emerged melt water is transferred to the uppermost ocean grid cell. Reaching a temperature below 0°C, precipitation becomes snow. When the accumulation of snow on sea-ice leads to submerging, the snow is converted to sea-ice with the result of a net heat gain, since the heat of snow fusion is higher than the one of sea-ice.

The relation between the interfaces of ocean/sea-ice and ocean/atmosphere can be expressed by

$$\rho_w c_w \Delta z_1 \frac{\partial \Theta_1}{\partial t} = (1 - I)Q_w + I(Q_{cond} - h_i \rho_i L_i)$$

where c_w is the specific heat capacity over water, Δz_1 the thickness and Θ_1 the temperature of the upper ocean layer and L_i the latent heat of the fusion of sea-ice.

For the undersurface is assumed, that when Θ_1 is below T_{freeze} , new sea-ice is formed and when Θ_1 exceeds the melting temperature, sea-ice will melt.

The effect of growth and melt influences the compactness of sea-ice in terms of increased compactness for freezing over water and decreased compactness for melting over thick sea-ice.

The salinity of sea-ice depends on the age. Multi-year sea-ice contains salt concentrations of about 3 psu (1psu = 1 g/kg water) on the contrary of much higher concentrations for thinner sea-ice. For the model the average concentration of 5 psu is assumed. The salt and fresh water exchange is considered by a varying salinity for the uppermost sea-ice layer [Marsland et al., 2003].

The atmospheric model ECHAM6 includes sea-ice in terms of providing surface temperature and albedo for each time step giving lower boundary conditions. For this sea-ice model it is assumed that the sea-ice thickness is constant for each time step and a new thickness is constantly applied. The existent balance between surface albedo, incoming atmospheric fluxes, conductive heat flux through snow and ice and outgoing long wave radiation is used to determine the sea-ice surface temperature [Notz et al., 2013].

3.2 Model Simulations with the MPI-ESM

3.2.1 CMIP5 Protocol for Decadal Simulations

The intention of CMIP5 is to define common model experiments that are run by multiple model groups to coordinate climate science research and to support IPCC assessments [Taylor et al., 2012]. More than 20 modeling groups contributed simulations to CMIP5 with overall more than 50 different model versions. These models consider coupled processes between ocean, atmosphere, ice and land and partly include components of the earth system. The framework of CMIP5 contains climate change model experiments on two timescales: long-term or century time scale and near-term decadal experiments covering time periods from 10-30 years [Taylor et al., 2012].

There is an uncertainty in estimating radiative forcing for the future. Representative concentration pathways (RCPs) describe possible future scenarios depending on possible future atmospheric composition. For this estimation all major anthropogenic greenhouse gases are considered [Meinshausen et al., 2011]. The projections include future population growth, technological development and possible reactions of society. CMIP5 provides four RCPs that differ in the amount of radiative forcing in year 2100 indicated by the labels. RCP8.5 complies with a radiative forcing of 8.5 W/m² by 2100 and is the worst assumed case among the four scenarios. RCP2.6 is called a peak-and-decay scenario because it reaches a maximum near 2050 before it decreases to a level of 2.6 W/m² being the most optimistic one. The RCP4.5 and RCP6.0 lie in the middle and represent the intermediate scenarios [Meinshausen et al., 2011]. For the CMIP5 decadal predictions (2006-2035) the RCP4.5 scenario is used considering that the RCPs for the time period until 2035 do not diverge on significant scales [Meehl et al., 2013].

Figure 3 gives a schematic overview of the CMIP5 decadal prediction experiments (from [Taylor et al., 2012]). This classification determines which simulations should be completed and which simulations are additional to examine specific aspects. The benefit of this evaluation is to enable model intercomparison and to archive a multimodel dataset for interpretation.

The “core” set representing the inner pink shaded circle are required for model evaluation. The surrounding yellow “tire” adds specific aspects concerning climate model forcing, response and processes to the evaluation. The core shows two different sets of near-term integration namely the 10-year and the 30-year hindcast and prediction ensembles.

Additional aspects are displayed in the tire like the expansion to a more frequent initialization (e.g. every year) both with more recent as well as earlier years. Reasons for that are the availability of salinity and ocean temperature data received from Argo floats since recent years and the statistical

benefit. Other possible integrations are the hindcast without volcanic eruptions, a hypothetical Pinatubo-like volcanic eruption in 2010, alternative initialization methods, the increase of CO₂-concentration of 1% per year and the integration of an atmospheric chemistry/pollutant experiment.

Typical for the CMIP5 long-term simulations is a several-hundred-year control simulation to calculate an equilibrium climate for preindustrial conditions. For the CMIP5 model integration is also the option of a 100-years control run introduced [Taylor et al., 2012].

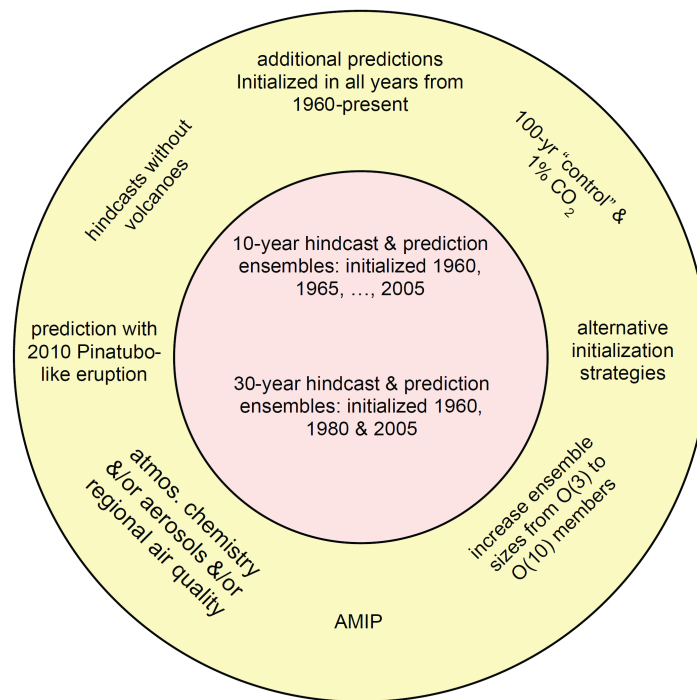


Figure 3: Schematic summary of CMIP5 decadal prediction integration

3.2.2 MPI-ESM Simulations

For this work the uninitialized hindcast and future projections as well as the initialized decadal hindcasts and predictions from the MPI-ESM-LR were analyzed, because the low-resolution module provides more ensemble members than the MPI-ESM-MR and because the differences in sea-ice extent between the MR and LR version are small [Hübner, 2013; Notz et al. 2013].

The uninitialized hindcasts of the MPI-ESM-LR run from 1850 until 2005 with three ensemble members which were extended by future projections (RCP4.5) until the year 2020 for this work. The decadal simulation from the MPI-ESM-LR are initialized every year covering the period from 1961-2010 with generally three ensemble members. Beginning 1966 and then every five years the simulations start with 10 ensemble members. The previously mentioned 30-year ensembles are generated by extension of three of the ten ensemble members beginning in 1961, 1981 and 2006.

Table 1 shows an overview of the CMIP5 decadal experiments that are available from the model MPI-ESM-LR during the 1996-2005 period. The orange highlights years when ten simulations were started. “decadal1995” is a file name running from 1996-2005 with ten ensemble members. The years before and after 1996 simulations were also started, thus there is a total of 47 ensembles running every year. For this work the 10 ensembles initialized 1996 are further analyzed (highlighted in red).

MIP-ESM-LR decadal simulations

| | 1996 | 1997 | 1998 | 1999 | 2000 | 2001 | 2002 | 2003 | 2004 | 2005 |
|---------------|------|------|------|------|------|------|------|------|------|------|
| File name | | | | | | | | | | |
| decadal1980 | 3 | 3 | 3 | 3 | 3 | 3 | 3 | 3 | 3 | 3 |
| decadal1981 | | | | | | | | | | |
| decadal1982 | | | | | | | | | | |
| decadal1983 | | | | | | | | | | |
| decadal1984 | | | | | | | | | | |
| decadal1985 | | | | | | | | | | |
| decadal1986 | 3 | | | | | | | | | |
| decadal1987 | 3 | 3 | | | | | | | | |
| decadal1988 | 3 | 3 | 3 | | | | | | | |
| decadal1989 | 3 | 3 | 3 | 3 | | | | | | |
| decadal1990 | 10 | 10 | 10 | 10 | 10 | | | | | |
| decadal1991 | 3 | 3 | 3 | 3 | 3 | 3 | | | | |
| decadal1992 | 3 | 3 | 3 | 3 | 3 | 3 | 3 | | | |
| decadal1993 | 3 | 3 | 3 | 3 | 3 | 3 | 3 | 3 | | |
| decadal1994 | 3 | 3 | 3 | 3 | 3 | 3 | 3 | 3 | 3 | |
| decadal1995 | 10 | 10 | 10 | 10 | 10 | 10 | 10 | 10 | 10 | 10 |
| decadal1996 | | 3 | 3 | 3 | 3 | 3 | 3 | 3 | 3 | 3 |
| decadal1997 | | | 3 | 3 | 3 | 3 | 3 | 3 | 3 | 3 |
| decadal1998 | | | | 3 | 3 | 3 | 3 | 3 | 3 | 3 |
| decadal1999 | | | | | 3 | 3 | 3 | 3 | 3 | 3 |
| decadal2000 | | | | | | 10 | 10 | 10 | 10 | 10 |
| decadal2001 | | | | | | | 3 | 3 | 3 | 3 |
| decadal2002 | | | | | | | | 3 | 3 | 3 |
| decadal2003 | | | | | | | | | 3 | 3 |
| decadal2004 | | | | | | | | | | 3 |
| Total running | 47 | 47 | 47 | 47 | 47 | 47 | 47 | 47 | 47 | 47 |

Table 1: Number of all ensemble members that are running during the time period 1996-2005 with the MPI-ESM-LR model. The lower row shows the total number of all ensembles running in each year.

Before the model can perform the simulations on given time periods, it has to be set in an equilibrium state by a spin-up procedure. This spin-up is started from simulated temperature and salinity fields of a CMIP3 preindustrial control experiment and is run in MPI-ESM-LR over 1900 years and in MPI-ESM-MR for about 1500 years. The benefit is to archive radiation balance and to minimize model trend. As a next step for the uninitialized simulations, a 1000 year control run under preindustrial conditions is implemented [Jungclaus et al., 2012]. In this way the trend of all sea-ice relevant parameters can be limited to less than 0.001% [Notz et al., 2013]. The uninitialized simulations are started from the receiving climate state and run under existing greenhouse and aerosol gas concentration for the historical period 1850 to 2005 and the RCP4.5 scenario later on.

For decadal simulations a MPIOM standalone experiment is used to nudge the model state towards three-dimensional ocean temperature and salinity anomalies taken from National Center of

Environmental Predictions (NCEP)/ National Oceanic and Atmospheric Administration (NOAA) reanalysis [Müller et al., 2012]. The spin-up for these simulations lasted only a few decades, thus the initial state is closer to the actual climatology [Jungclaus et al., 2012]. The ten year run of each ensemble member is always started on January 1st and an ensemble for each start year is created by a 1-daylagged initialization. An assimilation of atmospheric parameters is not conducted.

3.3 Evaluation and Verification Concept

3.3.1 Qualitative evaluation

In this work, the decadal simulations are qualitatively compared to the long-term simulations and to observations to start exploring the science question: do the initial conditions in the hindcast lead to more accurate retrospective predictions of sea-ice compared to the uninitialized simulations and if so, on what time scales?

The sea-ice observational data used in this work are based on different sources which are described in Hübner et al. (2013). The simulated sea-ice extent is compared to the AMSR-E dataset [Spreen et al., 2008], NSIDC data [Cavalieri et al., 1997] and the Hadley Centre Sea Ice and Sea Surface Temperature (HadISST, Rayner et al. [2003]) dataset.

3.3.2 Outlook Quantitative Evaluation for Follow-up Studies

The evaluation presented in this work can only start addressing the question about predictability of sea-ice in decadal simulations. Follow-up studies will need to assess and quantify skill through various quantitative measures. To estimate skill from the hindcasts, a verification framework similar to the one presented by Goddard et al. [2012] could be applied. This verification system declares standardization to observation data, verification metrics, hindcast period, ensemble size, spatial and temporal smoothing and graphical representation to maintain a level to compare different prediction systems. The elements used in this verification framework are generated from the US CLIVAR Working Group on Decadal Predictability and collaborators.

Decadal simulations are partly spatial and temporal smoothed to improve skill and enable comparison amongst different models. Through spatial smoothing the input of unpredictable grid-scale noise can be reduced. Temporal smoothing is accomplished by evaluating various time scales: year 1, years 2-5, years 6-9 and years 2-9. The different time scales display diverse statements and represent a minimum regarding skill depending on average and lead time. Since the simulations start at initialized conditions the first year is most predictable and can be compared to available seasonal-to-interannual predictions. The range between the years 2-5 and 6-9 shows the interannual timescale and can be compared giving evidence about the reliance on the processing time. The year 1 is not regarded in these timescales and the 2-9 timescale anymore because of the strong effect through initialization. The eight-year average containing year 2-9 stands for decadal-scale climate and is the general temporal scale for CMIP5 decadal prediction experiments [Goddard et al., 2012].

A bias is a function over time that emerges from different sources like initialization, imperfect representation of the natural and the interannual-to-multidecadal variability in the climate models, future radiative forcing and inaccurate observation data [Meehl et al., 2013]. A possibility to remove

the bias by initialization is shown in Figure 1, where the mean drift of each initialization is calculated and subtracted from each decadal hindcast. The resulting drift is depicted with dashed lines also color-coded with negative drift in the early time periods where the mismatch of observation and simulation of greater extent and positive drift later on. The accrued drift described here can be corrected by distinguishing initial time when considering the mean bias [Kharin et al., 2012].

4 Results

In this Chapter the results of this work are presented for the Arctic (Section 4.1) and the Antarctic (Section 4.2). Each section first compares the representation of sea-ice in the MPI-ESM uninitialized hindcast simulations to other CMIP5 models and to observations. In a second step the initialized hindcast and prediction experiments from the MPI-ESM are compared to the uninitialized hindcast and projection experiments from the MPI-ESM and to observations. A special focus of the analysis is on a set of hindcast simulations initialized in 1996 as an example.

4.1 Arctic Sea-ice

Figure 4 shows the timeseries of September mean sea-ice extent from 1960-2005 in million square kilometers for all climate models participating in CMIP5. Different ensemble members of the same model are marked with different line styles. Considering the multimodel ensemble as a whole, it represents an overall development of the climate system whose confidence can be evaluated with the model spread [Taylor et al., 2012]. Consistent with observations (black solid, dashed and dotted lines for NSIDC, HadISST and AMSRE respectively), all CMIP5 models show a downward trend which is also reproduced by the CMIP5 multi-model-mean (yellow). In the beginning of the time series, the range is between $3.2 \times 10^6 \text{ km}^2$ (GISS, MIROC) and $12.1 \times 10^6 \text{ km}^2$ (CSIRO). The multi-model-mean lies below the observations for the entire timeseries, especially during the time from 1978 when satellite observation started and the quality of observation data therefore improved. The MPI-ESM-LR (red bold lines) and the MPI-ESM-MR (blue bold lines) both running with three ensemble members lie mostly above the CMIP5-multi-model-mean and track down the real decline of sea-ice extent reasonably well (see also Hübner, 2013; Notz et al., 2013).

September Mean Arctic Sea Ice Extent

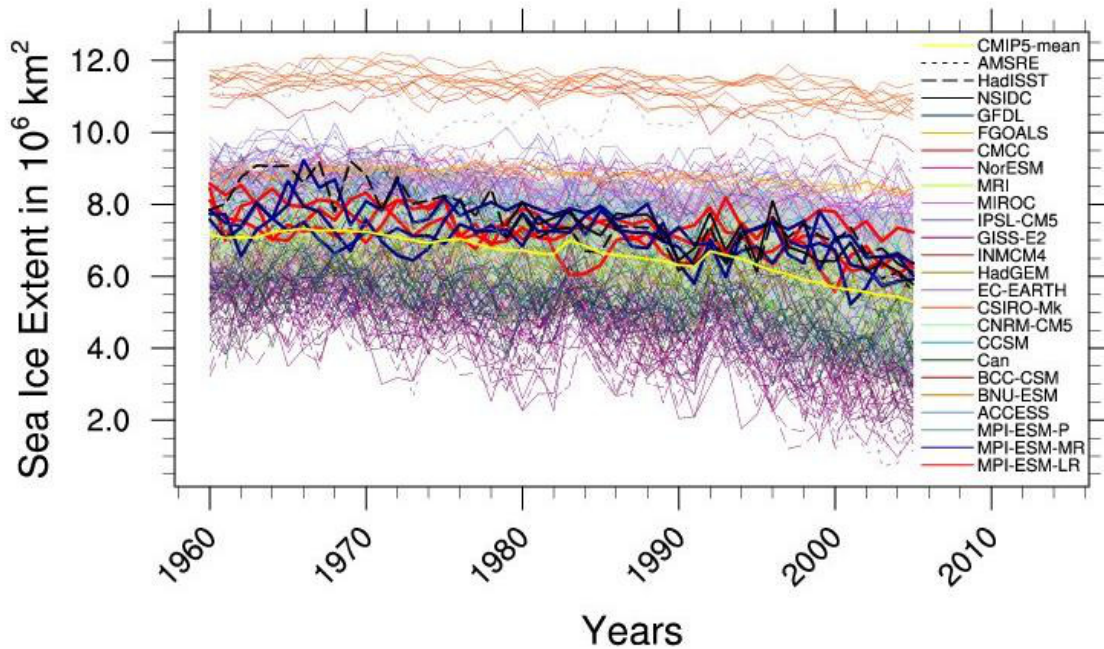


Figure 4: Timeseries (1960-2005) of September mean Arctic sea-ice extent from the uninitialized CMIP5 hindcast simulations compared to observations: NSIDC (1987-2011, black solid line), HadISST (1987-2011, black dashed line), and AMSR-E (2002-2011, black dotted line). Sea-ice extent is calculated as the total area of grid cells with a sea-ice concentrations of at least 15%. The MPI-ESM-LR (red) and MPI-ESM-MR (blue) simulations are shown in bold. The model mean over all model simulations is highlighted in yellow.

A further comparison is carried out by looking at the annual mean of the uninitialized hindcast experiments for all the CMIP5 models and observations (Figure 5). Observations contain data from NSIDC (black solid line) and HadISST (black dashed line). The dataset of AMSR-E is not included, because the data does not cover this time interval. The climatological mean is created by evaluating the monthly average for each ensemble member of each model over the time interval 1986-2005 (upper panel) and 1996-2005 (lower panel). The seasonal cycle for the Arctic is clearly depicted by all models, showing the minimum sea-ice extent is reached in September at the end of the melting season and the maximum in March. Although the averaging period in the lower panel is ten years shorter, the results are very similar. The ensemble spread with around $9 \times 10^6 \text{ km}^2$ is about the same magnitude in March than in September. This spread is very large particularly because of questionable performance of the model BNU-ESM that simulates a very low sea-ice extent in winter, in contrast to the very high values simulated by MIROC and IPSL-CM5. The large spread in the summer months is mainly caused by the model CSIRO-Mk as already noted in Figure 4. The MPI-ESM also shows good performance in the annual cycle compared to observations (see also Hübner, 2013; Notz et al., 2013). The three ensemble members of the MPI-ESM-LR (red bold line) and MPI-ESM-MR (blue bold line) show the same annual cycle, matching observations better in the summer months than in winter with a slight underestimating of the sea-ice extent maximum.

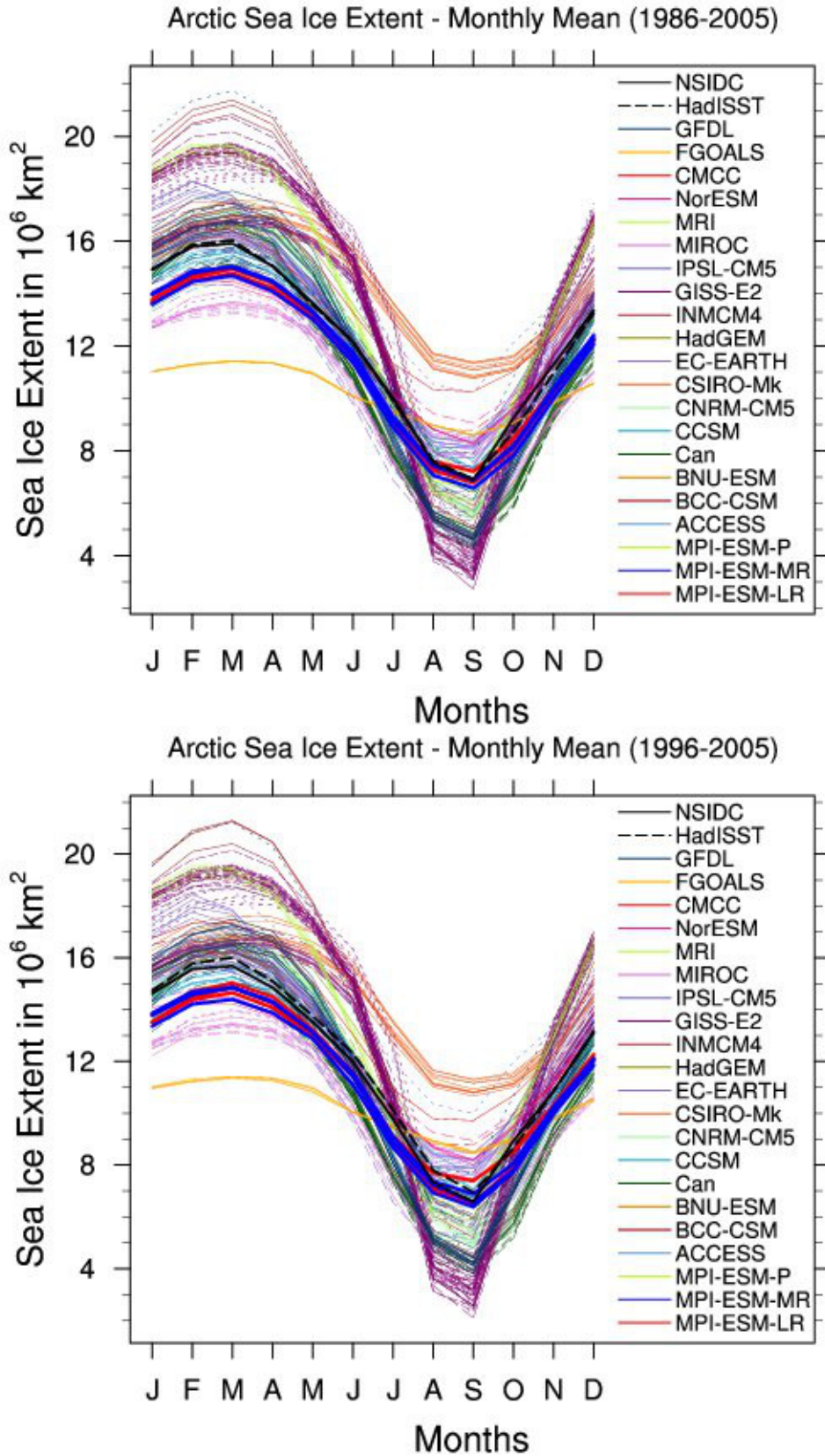


Figure 5: Mean seasonal cycle in sea-ice extent in the Northern Hemisphere averaged over 1986-2005 (upper panel) and 1996-2005 (lower panel) as simulated by the CMIP5 models compared to observations. The MPI-ESM-LR (red) and MPI-ESM-MR (blue) simulations are shown in bold. The black lines show observations from NSIDC (solid) and HadISST (dashed), respectively.

Figure 6 shows the timeseries from 1961-2020 of September mean Arctic sea-ice extent in km² from the initialized simulations of the MPI-ESM-LR (upper panel) and MPI-ESM-MR (lower panel) compared to observations (black). The initialized decadal simulations are color coded, with each color representing 5-6 initial years. The simulations were run each for ten years with an exception in the years 1961, 1981 and 2006 when three of the ten ensemble members were extended by additional 20 years receiving a total run of 30 years. Simulations initialized after the year 2005 are predictions forced by the RCP4.5. This MPI-ESM-LR provides three ensemble members initialized every year and ten ensemble members every five years. For most of the years the total of ensemble members accounts to 47 (see also Table 1). A general downward trend from both observations and simulations is indicated. In the beginning of the timeseries the decadal simulations overestimate the decline of sea-ice extent. It has to be noted, that satellite observation started in 1978 thus the quality of observation data should not be regarded inerrant. From 1979 onward the range of decadal simulations matches observations pretty well until around the year 2000 when observations decrease on a larger range and simulations underestimate the decline in general. It is apparent that some of the ensemble members track down the intensified drop of sea-ice extent. This short timescale has no potential though, to determine whether this trend is due to a more rapid change in the climate system or natural variability. The MPI-ESM-MR version starts with three ensemble members every five years until 2000 when the initialization occurs every year. Although having fewer ensemble members than the MPI-ESM-LR, the results of the two different model versions are very similar.

Besides the comparison to observations, Figure 7 shows a comparison of the decadal simulations to the uninitialized hindcasts and projections of the MPI-ESM-LR (upper panel) and MPI-ESM-MR (lower panel) for the September mean sea-ice extent timeseries. The projections begin in 2005 and are forced by the RCP4.5. On the upper panel the three ensemble members of the free-running MPI-ESM-LR simulations (red) fall in the same range as the decadal simulations (green). From 2005 onward the uninitialized projections lie over the observations even though one of the ensemble members represents the strong decline. In the lower panel, the free-running (blue) and initialized (orange) simulations from the MPI-ESM-MR show similar performance and match the overall trend shown from observations (black lines).

Overall, Figure 6 and 7 show that the quality of MPI-ESM-LR and MPI-ESM-MR is comparable for September sea-ice extent. Therefore, only the MPI-ESM-LR is used for remaining comparisons in the Arctic, since it has more ensemble members. They also indicate that from this qualitative comparison there is no big difference between the initialized and uninitialized simulations.

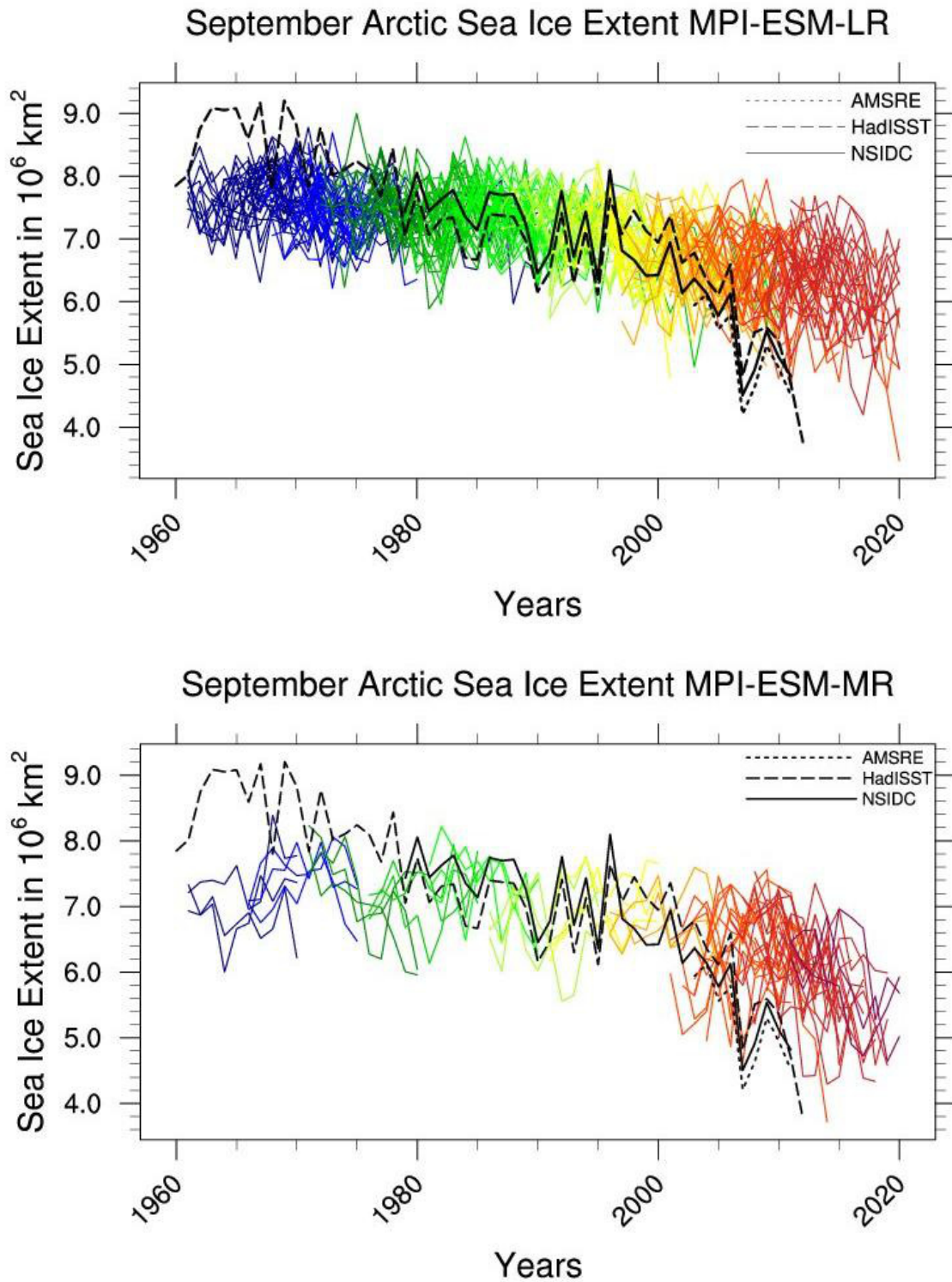


Figure 6: Timeseries (1960-2020) of September Arctic sea-ice extent from the MPI-ESM-LR (upper panel) and the MPI-ESM-MR (lower panel) initialized decadal simulations compared to observations (black). The model simulations are color coded, with each color combining initial years of the simulations that each run for 10 years. The decadal predictions cover the time period 2006-2020, following the RCP 4.5 scenario.

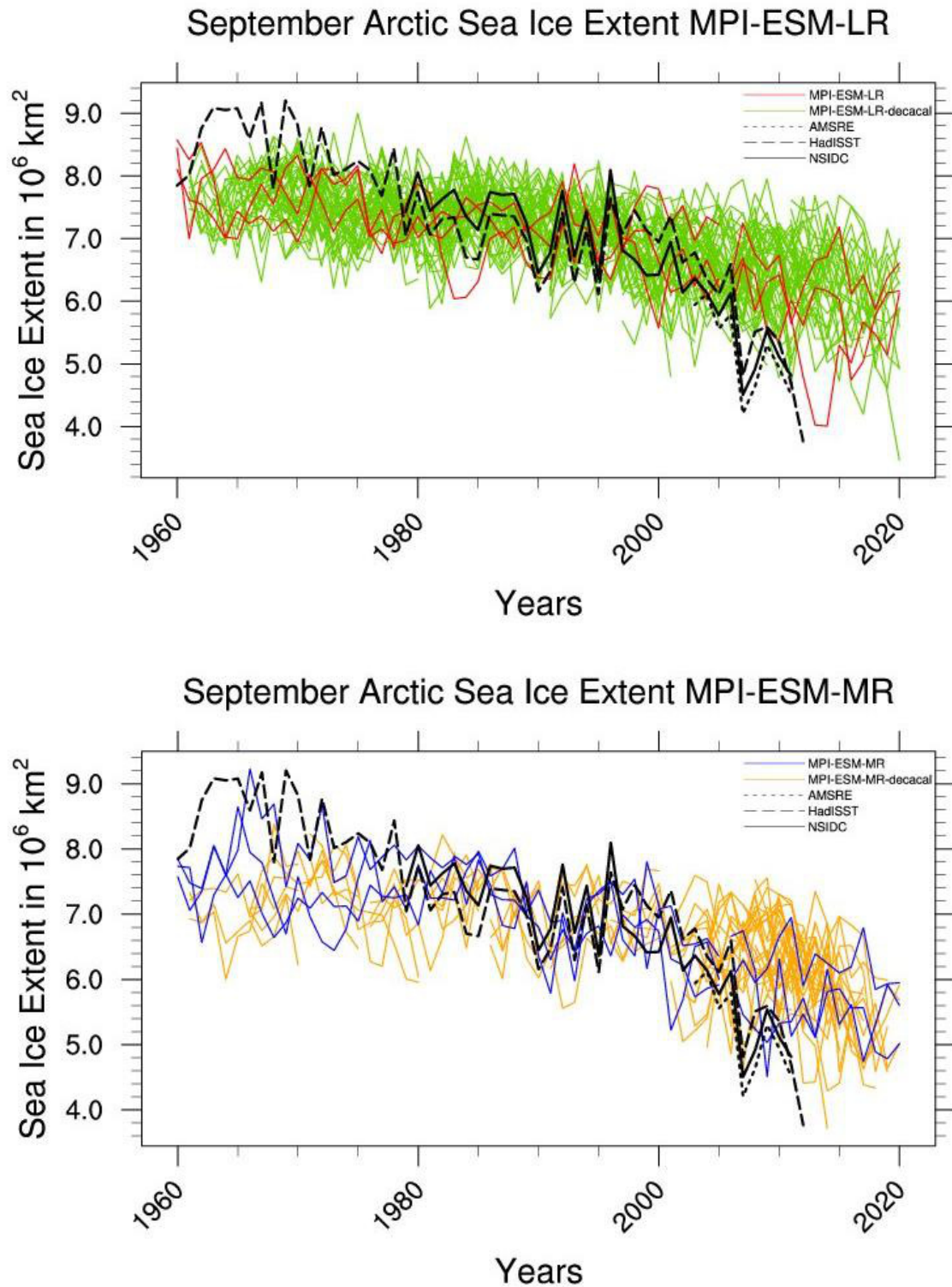


Figure 7: As Figure 6, but showing the initialized decadal simulations compared to the uninitialized simulations from the MPI-ESM-LR (upper panel) and the MPI-ESM-MR (lower panel) compared to observations (1960-2020).

As already mentioned in Section 3.4.2, decadal simulations depend on their lead time. Figure 8 shows four panels each covering different time horizons of the annual cycle of September mean sea-ice extent. For this evaluation the set of ten ensemble members initialized in 1996 from the MPI-ESM-LR is chosen (highlighted red in Table 1). From top left to bottom right the lead times are one year, year 2-5, year 6-9 and the years 2-9, following the grouping of lead times suggested by the verification approach of Goddard et al. (2012). The annual cycle over the initial year 1996 shows the largest differences between observation data, decadal and long-term simulations. The summer is better represented by the decadal hindcasts. In winter one ensemble member of the uninitialized simulations matches the observation and also the mean outperforms decadal scales. The initial year is left out in the other panels, because the “initialization shock” might influence the trend on following years. It should however be noted that due to natural variability the sea-ice distribution in the long-term free-running simulation is not meant to be in agreement with the one observed in a particular year. Rather this agreement should only hold in a climatological sense as shown in the previous figures. The spread in the other panels is smaller. Comparing the lead times 2-5 and 6-9 there is hardly any difference. Uninitialized runs lie in the range of the standard deviation of the initialized simulations and are slightly lower / higher than observations during winter / summer, respectively. This can also be seen in the last panel spanning the period 1997-2004.

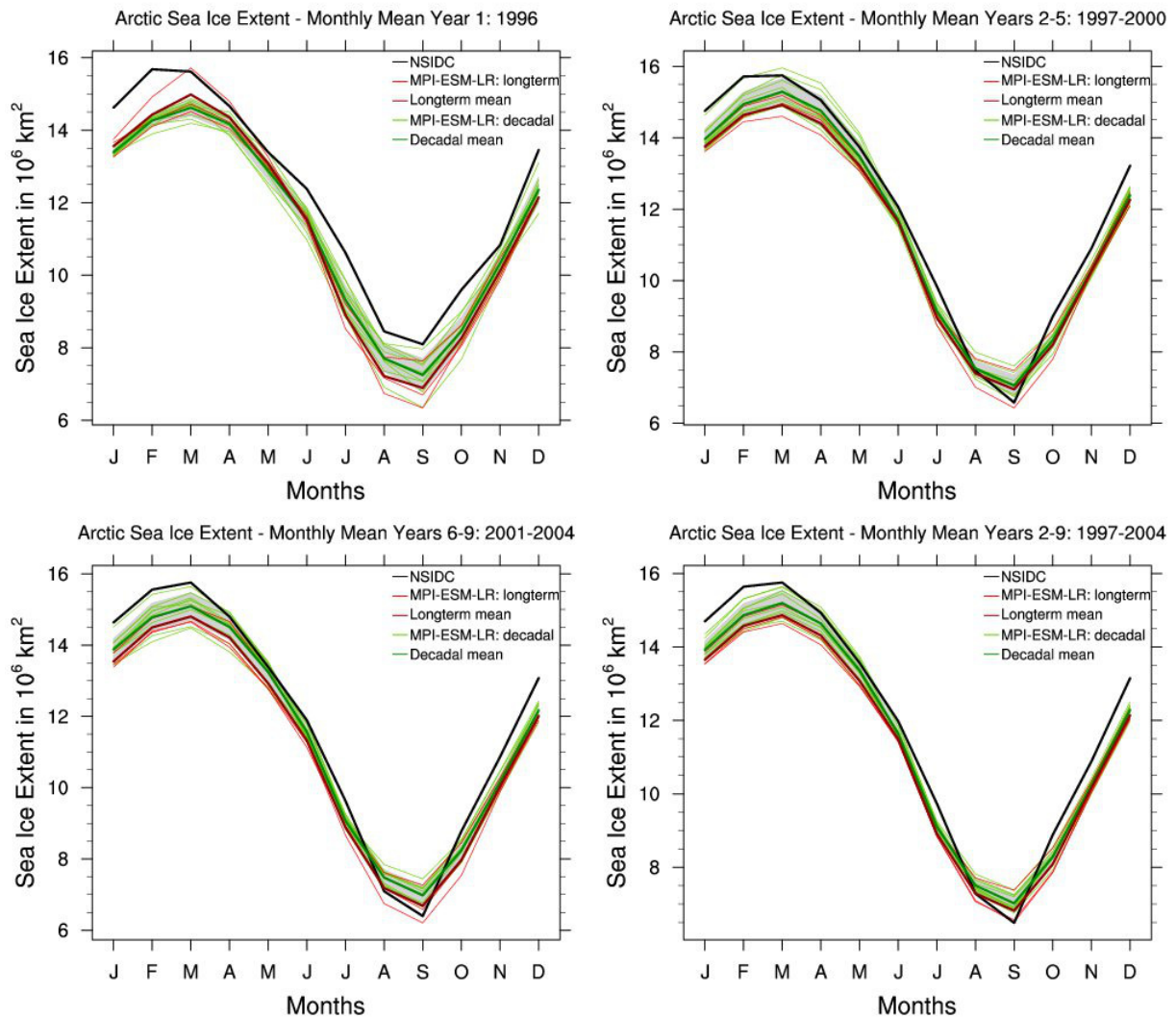


Figure 8: Seasonal cycle in Arctic sea-ice extent of the 10 ensemble members of the MPI-ESM-LR decadal simulations that are all started in 1996 compared to NSIDC observations and the uninitialized MPI-ESM-LR simulations. The individual panels show 1996 (lead time 1 year, upper left), 1997-2000 (lead time 2-5, upper right), 2001-2004 (lead time 6-9, lower left), and 1997-2004 (lead time 2-9, lower right), see text for details.

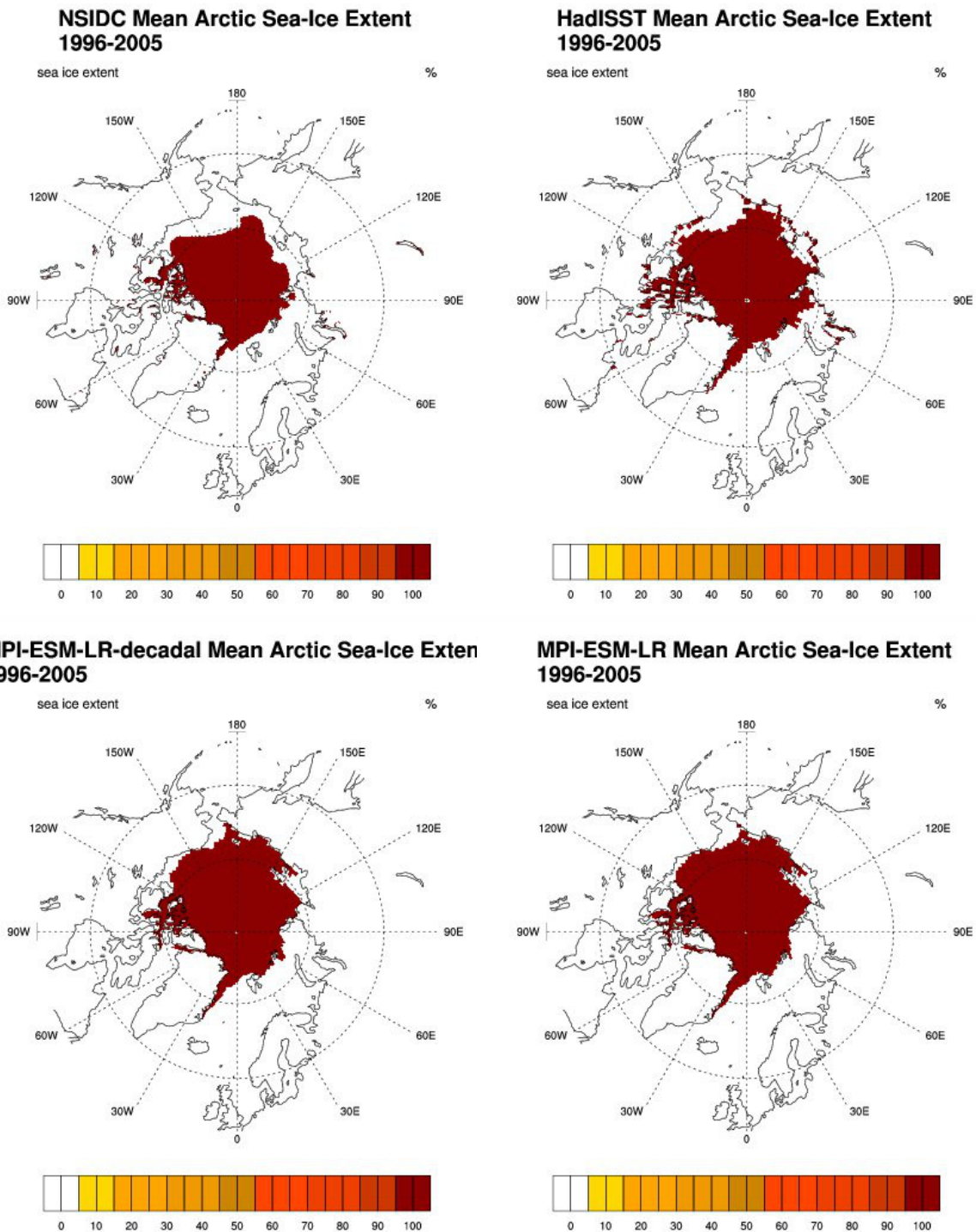


Figure 9: Polar stereographic projection of mean Arctic September sea-ice extent averaged over the period 1996-2005 for NSIDC (upper left), HadISST (upper right), the 10-ensemble mean of the initialized MPI-ESM decadal simulations that were started in 1996 (lower left), and the 3-ensemble mean of the MPI-ESM-LR uninitialized simulation (lower right). Sea-ice concentrations in this figure are set to 100% once the concentration exceeds the 15% threshold that is used for the sea-ice extent calculation.

To determine regions with possibly more or less predictive skill, the geographical distribution is depicted in Figure 9. The polar stereographic projections show the climatological mean (1995-2005) sea-ice extent. The first row shows NSIDC (left) and HadISST (right) and the second row shows the ensemble means of the 10-ensemble members from the initialized simulations (left) and of the 3-ensemble members from the uninitialized hindcasts (right). The remarkable similarity between initialized and uninitialized simulations as already assessed in previous figures can also be seen in this plot. The panels for the MPI-ESM show hardly any difference, see also Figure 10 that shows the differences for the long-term simulations (left) and decadal simulations (right) to the NSIDC dataset. Generally the spatial pattern of the simulations matches the observed patterns very well. In the Kara Sea observations show more sea-ice extent than the uninitialized and initialized simulations. Slightly larger sea-ice cover than observed is simulated in the East Siberian Sea and Beaufort Sea. Striking is the difference between data of NSIDC and HadISST. HadISST shows a larger sea-ice extent especially at the east coast of Greenland, the Queen Elisabeth Islands, the Beaufort Sea and around the Siberian coast line. These differences need to be accounted for in model evaluation and verification systems. A reason for the bias may be the differences in simulated and observed sea surface temperatures [Hübner, 2013].

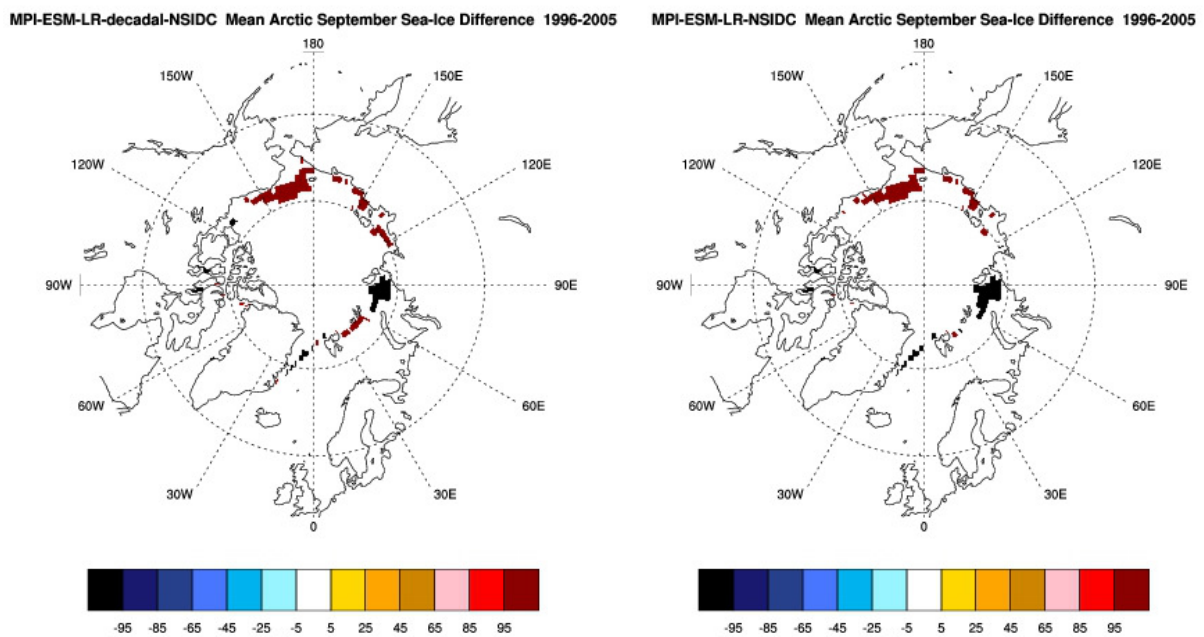


Figure 10: Polar stereographic projection of the differences in climatological mean (1996-2005) September mean Arctic sea-ice extent between (left) the MPI-ESM-LR 10-ensemble mean initialized simulations and NSIDC observations and (right) the 3-ensemble mean uninitialized simulations and NSIDC observations. Sea-ice concentrations are set to 100% once the concentration exceeds the 15% threshold that is used for the sea-ice extent calculation, why relative differences are either + or - 100%.

4.2 Antarctic Sea-ice

In this Section results are presented in a similar way to the Arctic (Section 4.1) but for Antarctic sea-ice.

The Antarctic has its minimum sea-ice cover in March with approximately four million square kilometers in the year 2000 which is around three million square kilometers smaller than in the Arctic. Also the observed trend over the recent decades differs from the one in the Arctic being substantially smaller in the Antarctic [Cavalieri and Parkinson, 2008].

The CMIP5 ensemble mean March Antarctic sea-ice extent (yellow) shows a small trend over the period 1960-2005 in agreement with observations (Figure 11). The CMIP5 ensemble mean lies around $3 \times 10^6 \text{ km}^2$ slightly underestimating observed sea-ice extent. While the observations from NSIDC and AMSR-E match each other, observations from HadISST are slightly higher. The MPI-ESM underestimates the amount of sea-ice extent with a bias of about $3.5 \times 10^6 \text{ km}^2$ (see also Hübner, 2013). On the other hand models like CCSM and CSIRO clearly overestimate sea-ice extent lying outside the standard deviation which is shaded in grey. Just a few models succeed in representing the real evolution of sea-ice like the MRI. A reason for the general underestimation of the sea-ice extent by most models, pointing to a systematic bias, might be a warm bias in the Antarctic region, but other factors might impact as well (see Chapter 1).

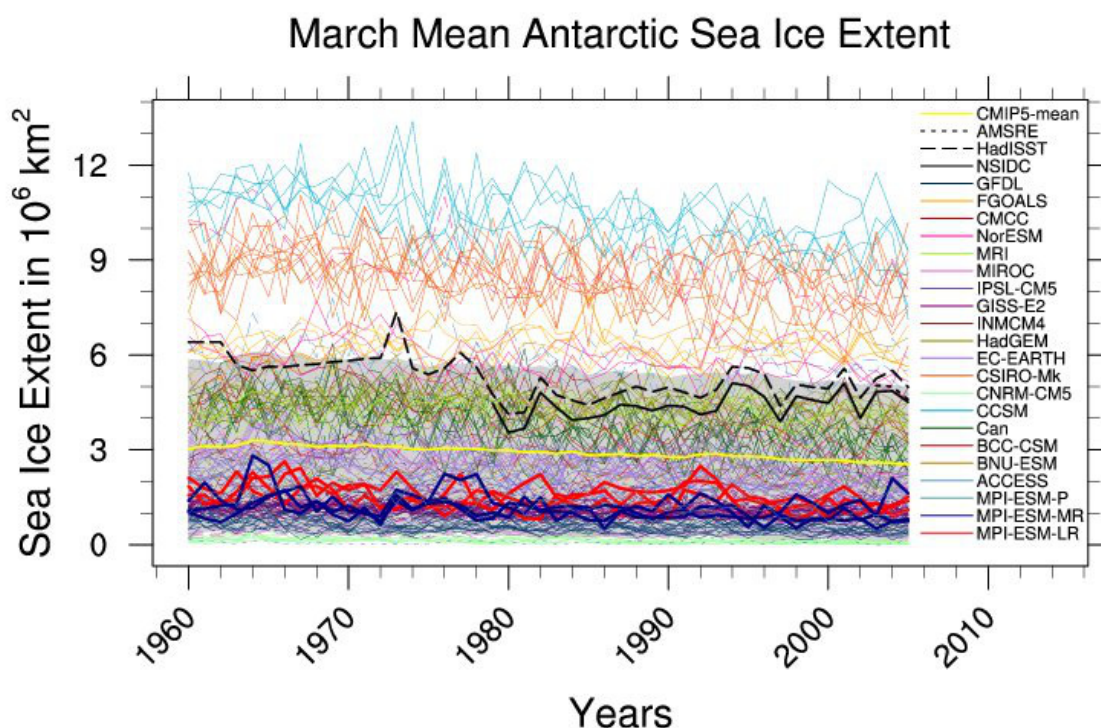


Figure 11: Timeseries (1960-2005) of March Antarctic sea-ice extent from the uninitialized CMIP5 hindcast simulations compared to observations: NSIDC (1987-2011, black solid line), HadISST (1987-2011, black dashed line), and AMSR-E (2002-2011, black dotted line). Sea-ice extent is calculated as the total area of grid cells with a sea-ice concentrations of at least 15%. The MPI-ESM-LR (red) and MPI-ESM-MR (blue) simulations are shown in bold. The model mean over all model simulations is highlighted in yellow.

The annual cycle of the individual CMIP5 models and the ensemble mean is displayed in Figure 12 with monthly averages of the sea-ice extent over the periods 1986-2005 (upper panel) and 1996-2005 (lower panel). The three ensemble members from the uninitialized free-running hindcast experiments by MPI-ESM-LR and MPI-ESM-MR are highlighted with bold red and blue lines, respectively. The seasonal cycle is clearly recognizable in all models with the maximum of sea-ice cover in September and the minimum in March. Regarding the ensemble of all the model simulations, the spread among different simulations for the minimum sea-ice extent is comparable to the one in the Arctic. At the maximum in the respective winter months the spread in the Antarctic is around $24 \times 10^6 \text{ km}^2$ difference which is distinctly larger than in the Arctic. For this evaluation the model HadGEM was not considered, because this single ensemble member overestimates the observed extent by around 60%. The annual cycle of Antarctic sea-ice extent is very well represented by the MPI-ESM simulations. As already mentioned before though, the model underestimates quantitative the observed value as is also seen for most of the other CMIP5 models.

Figure 13 shows the timeseries from 1960-2020 of March mean sea-ice extent. The upper panel displays decadal hindcast (until 2005) and prediction (from 2006 onward) simulations of the MPI-ESM-LR, the lower from the MPI-ESM-MR. Predictions are forced by the RCP4.5 scenario. These simulations are color-coded where each color represents a set of simulations depending on initial years. Observations are displayed in bold black lines with varying dashed pattern for NSIDC, AMSR-E and HadISST. In these plots the difference between observations and the MPI-ESM simulations becomes again evident (\sim two million square kilometers). Observations show a high internal variability of sea-ice extent that is equally present in the decadal simulations. The simulations reveal a slight downward trend. As for the Arctic, also for the Antarctic the performance of MPI-ESM-LR and MPI-ESM-MR is analogous.

Analog to Figure 13, Figure 14 contains the timeseries for sea-ice extent in March with the same observations (black) and decadal simulations. In addition the uninitialized simulations for the MPI-ESM-LR (upper panel) and MPI-ESM-MR (lower panel) are depicted. The uninitialized simulations lie generally in the same range as the initialized simulations and are therefore also distinctly too low. In the upper panel the initialized decadal simulations (red) show slightly higher values than the uninitialized (green) at the beginning around 1960. In progress the amplitude for these simulations is also higher. This aspect is distinctly displayed in the lower panel with simulations from the MPI-ESM-MR where one ensemble member of the free-running simulations (blue) reaches values of almost $3 \times 10^6 \text{ km}^2$ around 1965 and $2 \times 10^6 \text{ km}^2$ between 1975 and 1980. In the time period of projections from 2005 onward the amplitudes are remarkable smaller.

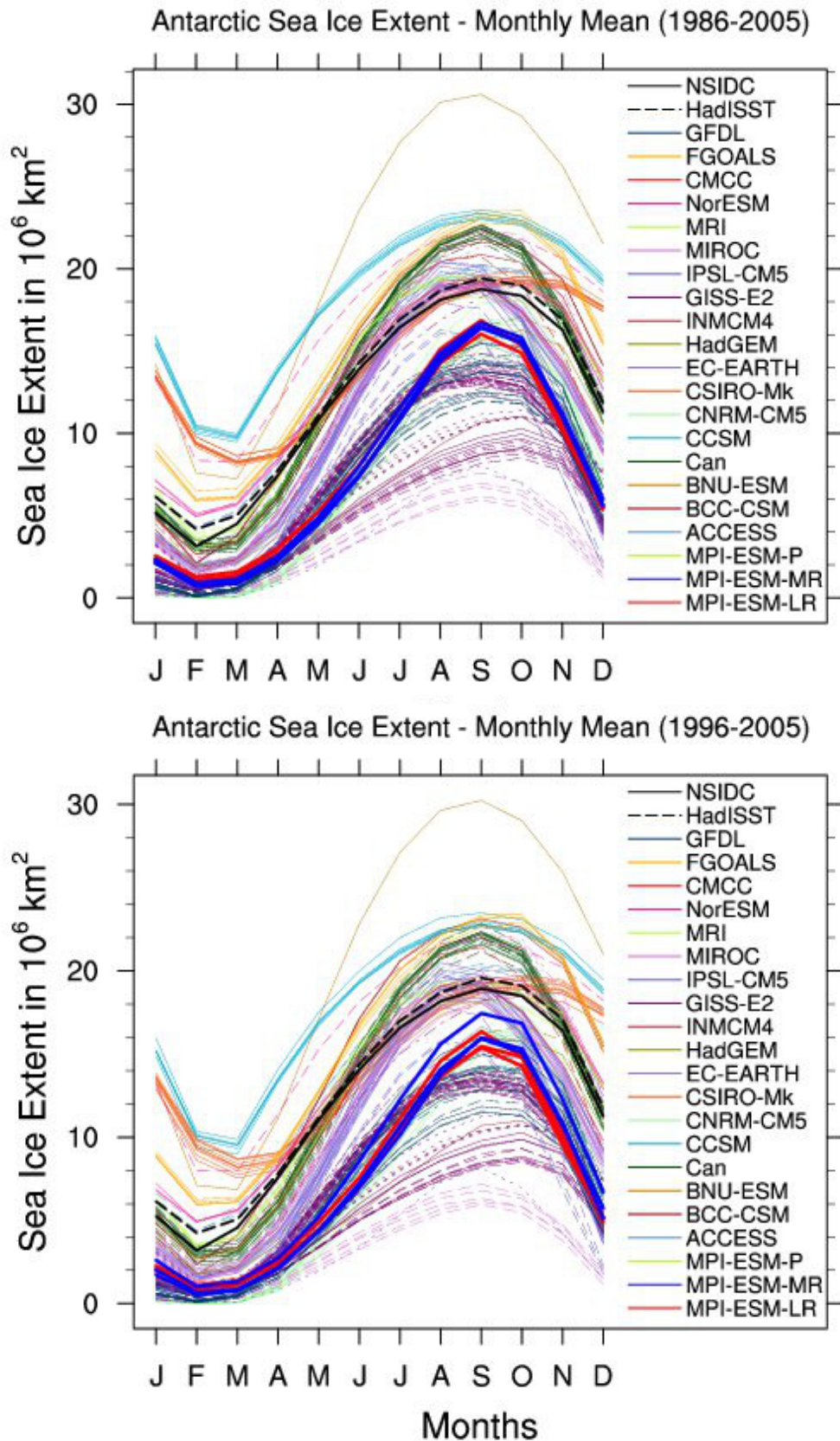


Figure 12: Mean seasonal cycle in sea-ice extent in the Southern Hemisphere averaged over 1986-2005 (upper panel) and 1996-2005 (lower panel) as simulated by the CMIP5 models compared to observations. The MPI-ESM-LR (red) and MPI-ESM-MR (blue) simulations are shown in bold. The black lines show observations from NSIDC (solid) and HadISST (dashed), respectively.

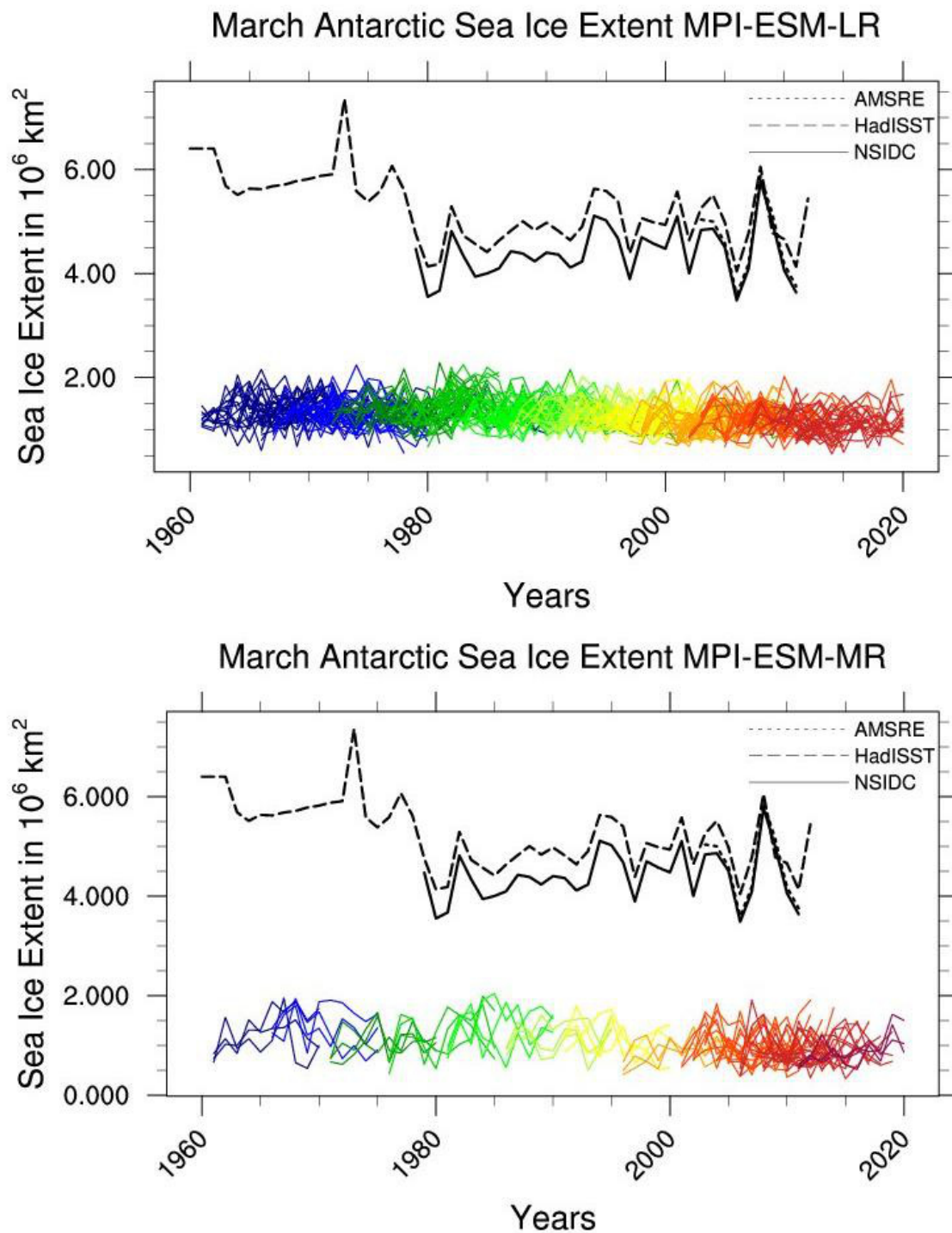


Figure 13: Timeseries (1960-2020) of March Antarctic sea-ice extent from the MPI-ESM-LR (upper panel) and the MPI-ESM-MR (lower panel) initialized decadal simulations compared to observations (black). The model simulations are color coded, with each color showing a different start year of the simulations that each run for 10 years. The decadal predictions cover the time period 2006-2020, following the RCP 4.5 scenario.

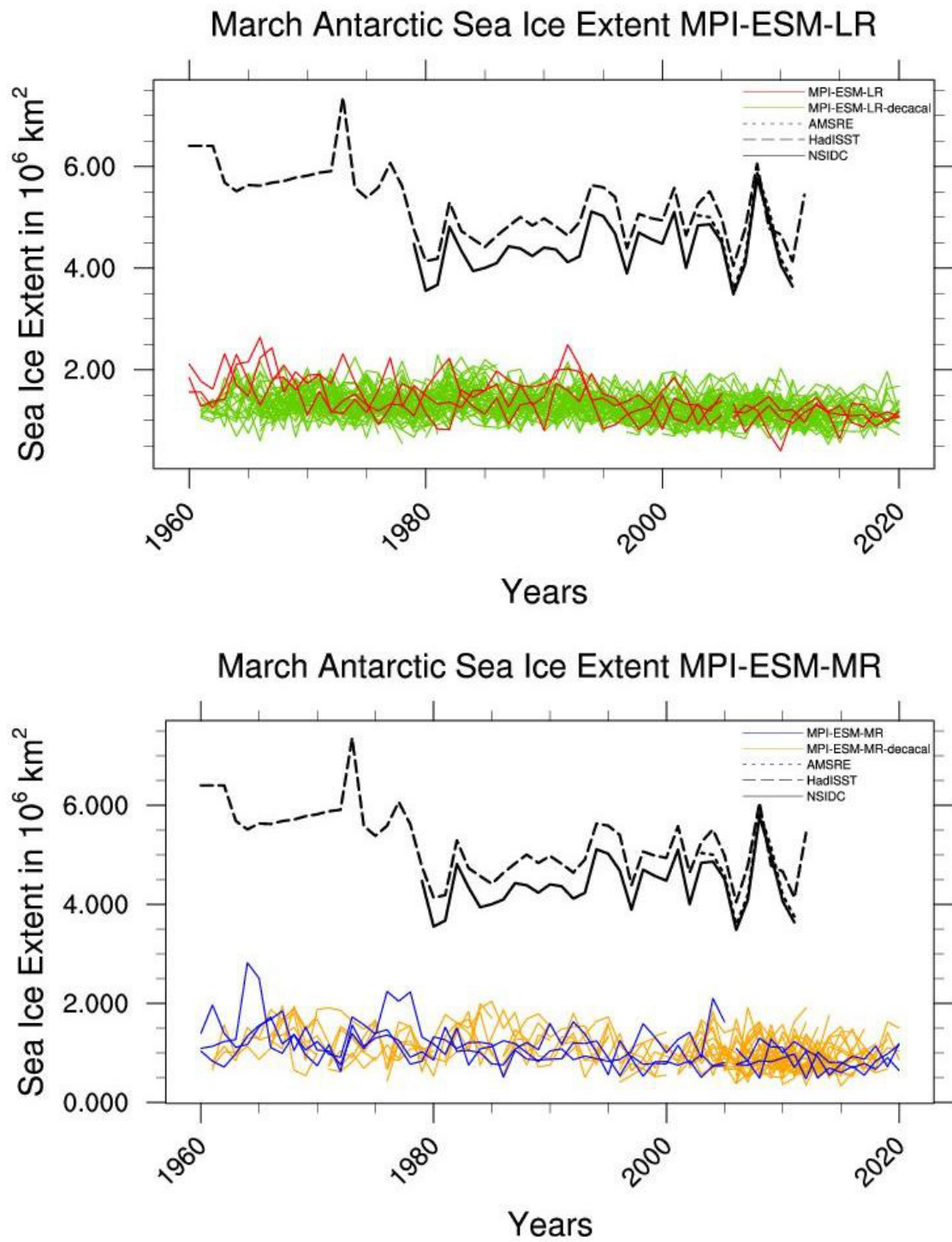


Figure 14: As Figure 13, but showing the initialized decadal simulations compared to the uninitialized simulations from the MPI-ESM-LR (upper panel) and the MPI-ESM-MR (lower panel) compared to observations (1960-2020).

Figure 15 shows the annual cycle of ten ensemble members from the decadal simulations starting 1996 and running for 10 years. The four panels show the progress on different lead times. All the panels show a constant bias in all months between simulations and observations. As seen before, the sea-ice extent is underestimated by the simulations. Regarding just the year 1996 (upper left) the simulations in winter have the widest range since two of the three uninitialized ensemble members are significantly closer to observations. In summer both initialized and uninitialized hindcasts do converge at the same level. This aspect can also be seen on the other panels. Differences between simulations can only be seen around September. Lead time 2-5 (upper right) shows the smallest range of the decadal simulations. On the decadal timescale from 1997-2004 (lower right) the ensemble means of uninitialized and initialized runs show exactly the same behavior.

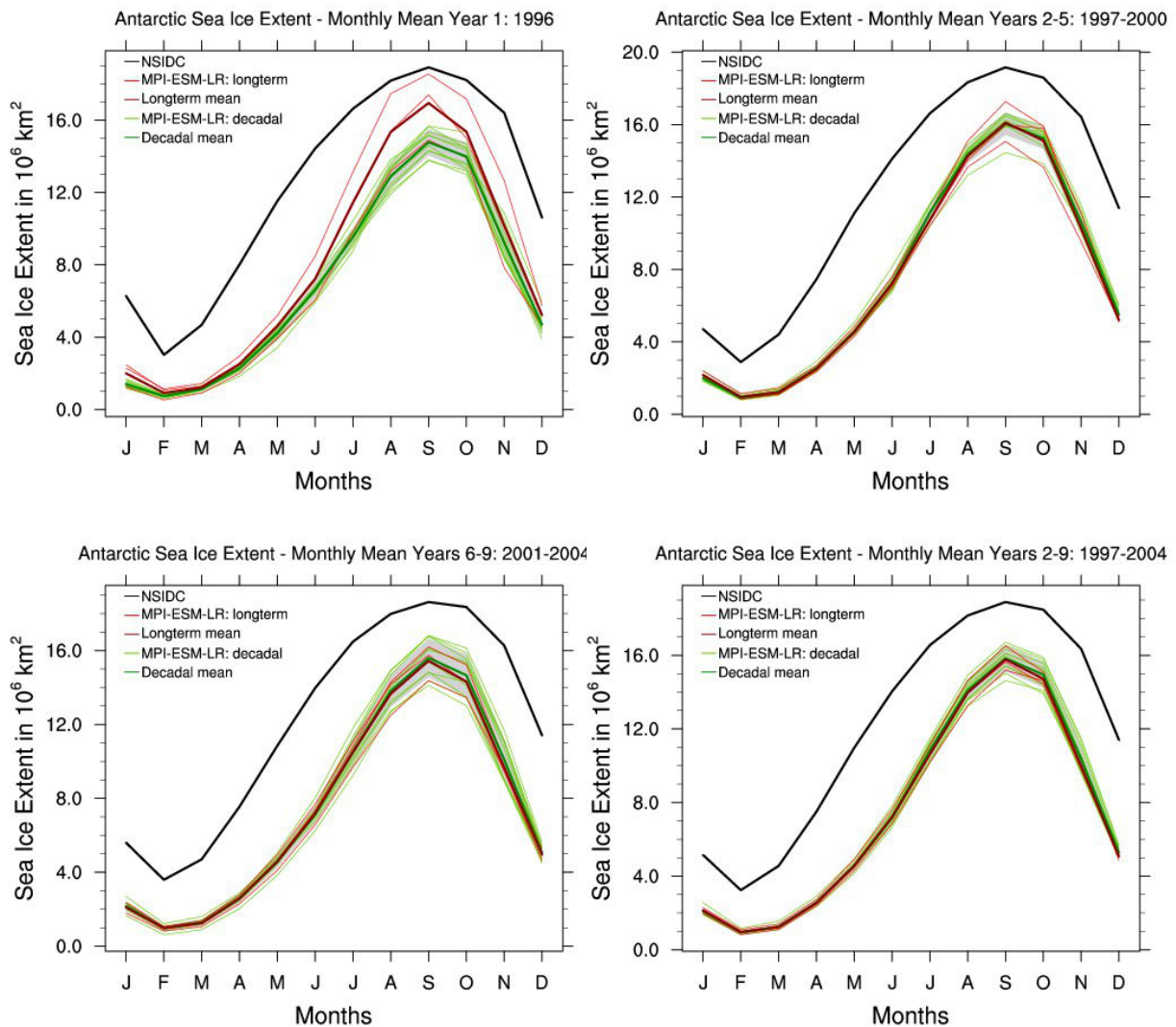


Figure 15: Seasonal cycle in Antarctic sea-ice extent of the 10 ensemble members of the MPI-ESM-LR decadal simulations that are all started in 1996 compared to NSIDC observations and the uninitialized MPI-ESM-LR simulations. The individual panels show 1996 (lead time 1 year, upper left), 1997-2000 (lead time 2-5, upper right), 2001-2004 (lead time 6-9, lower left), and 1997-2004 (lead time 2-9, lower right), see text for details.

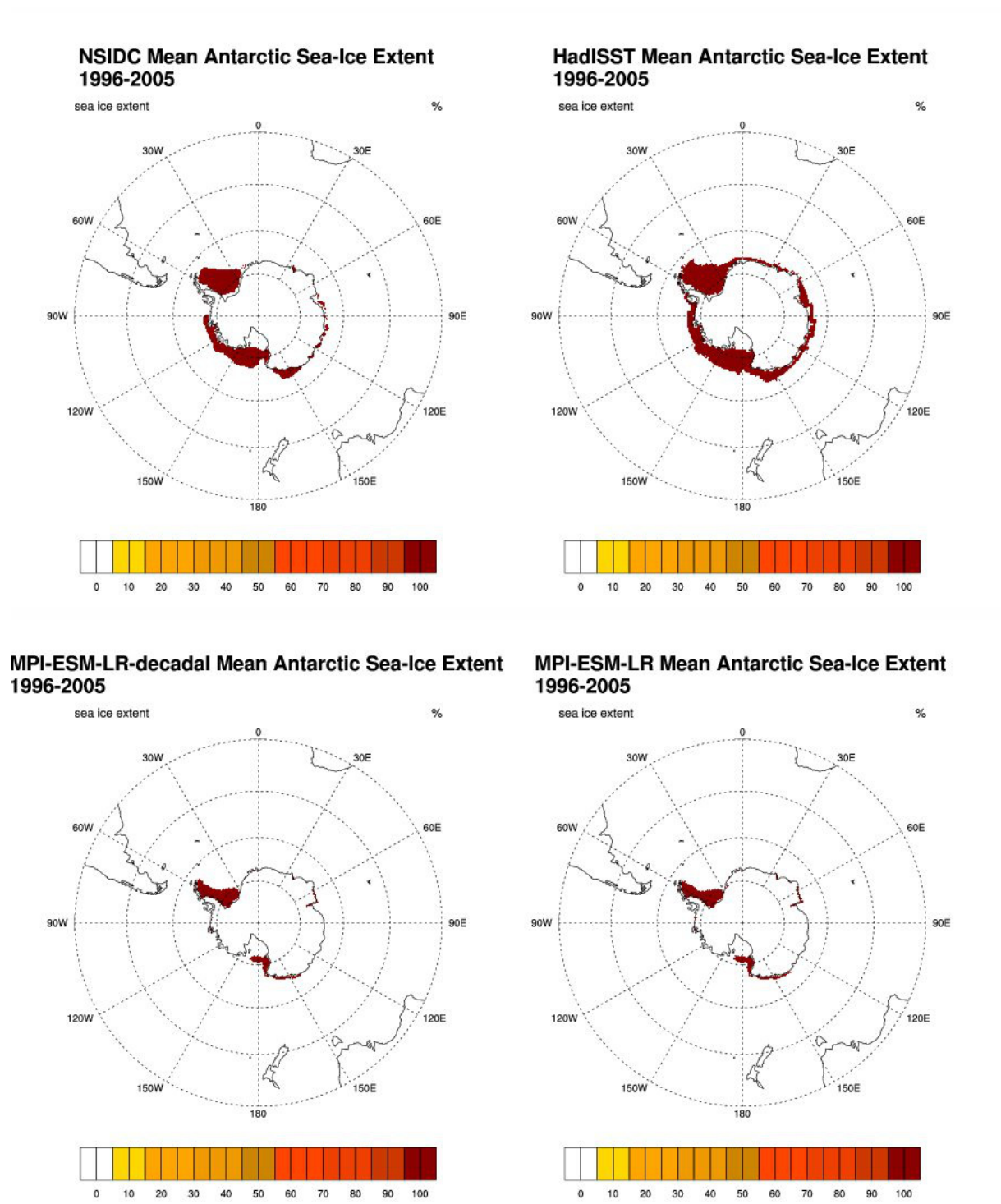


Figure 16: Polar stereographic projection of mean Antarctic March sea-ice extent averaged over the period 1996-2005 for NSIDC (upper left), HadISST (upper right), the 10-ensemble mean of the initialized MPI-ESM decadal simulations that were started in 1996 (lower left), and the 3-ensemble mean of the MPI-ESM-LR uninitialized simulation (lower right). Sea-ice concentrations in this figure are set to 100% once the concentration exceeds the 15% threshold that is used for the sea-ice extent calculation.

Overall, the previous investigation reveals that the MPI-ESM underestimates sea-ice extent in the Antarctic both in the uninitialized and in the initialized simulations, see also Figure 16 and 17. Especially regions in the Ross Sea, Amundsen Sea and the Weddel Sea show less sea-ice cover. However, also the observations differ among each other, with NSIDC observing distinctly less sea-ice cover than the observation from HadISST all around Antarctica, although these differences are much smaller.

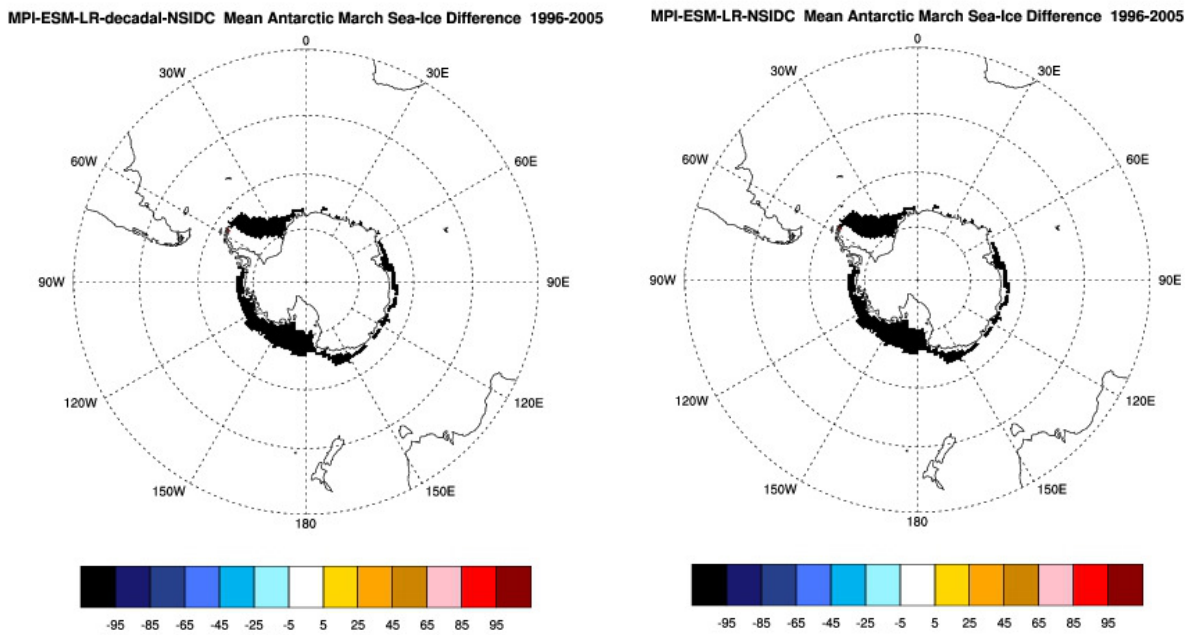


Figure 17: : Polar stereographic projection of the differences in climatological mean (1996-2005) March mean Antarctic sea-ice extent between (left) the MPI-ESM-LR 10-ensemble mean initialized simulations and NSIDC observations and (right) the 3-ensemble mean uninitialized simulations and NSIDC observations. Sea-ice concentrations are set to 100% once the concentration exceeds the 15% threshold that is used for the sea-ice extent calculation, why relative differences are either + or – 100%.

5 Summary and Outlook

The goal of this work was to compare the representation of sea-ice in initialized decadal predictions of the Max-Planck-Institute – Earth System Model (MPI-ESM) to uninitialized free-running hindcasts from this model and to observations. Decadal predictions are a new type of simulations that were included in the Coupled Model Intercomparison Project Phase 5 (CMIP5) experiment protocol. In contrast to long-term simulations that are run by global Earth system models (ESMs) to project future climate under various forcing scenarios, the decadal short-term (~10-30 years) simulations aim at predicting some aspects of slow natural variability by initializing the simulations from an observed climate state.

The MPI-ESM provides two versions, one low-resolution version (MPI-ESM-LR) and one mixed-resolution model (MPI-ESM-MR) that were both included in this work. For observations the datasets from AMSR-E (Advanced Microwave Scanning Radiometer – Earth Observing System), NSIDC (National Snow and Ice Data Center) and HadISST (Hadley Centre Sea Ice and Sea Surface Temperature) were used. The uninitialized hindcast predictions were assembled with other CMIP5 by comparing the minimum sea-ice extent for the time period 1960-2005 and the annual cycle of sea-ice extent for the period 1986-2005. The sea-ice extent is the sum of all grid cells, that are covered with sea-ice concentrations of at least 15%. The evaluation of decadal simulations was accomplished by a comparison of the decadal hindcasts and predictions to the uninitialized simulations and observations. Both experiments exceeding the historical time period until 2005 are forced with the RCP4.5 scenario. In addition a set of ten ensemble members from the MPI-ESM-LR initialized in 1996 is selected for further evaluation. This work is clearly divided into the evolution for the Arctic and Antarctic.

In the Arctic, all the uninitialized CMIP5 climate models show a downward trend in September mean Arctic sea-ice extent over the period 1960-2005 in agreement with observations, and the seasonal cycle is well represented by all models. Even though, a remarkable spread between the different models exists. The uninitialized simulations of the MPI-ESM-LR and MPI-ESM-MR track down the observed evolution of sea-ice extent well. A qualitative comparison between the long-term uninitialized and the decadal initialized simulations shows similar results in terms of trends, the annual cycle and spatial distribution of September Arctic sea-ice extent. The simulated quality of sea-ice extent is significantly less in the Antarctic compared to the Arctic. Most of the CMIP5 models including the MPI-ESM underestimate the sea-ice extent. In agreement with observations, a small trend is simulated and the observed high variability is also well reproduced by both the decadal and the long-term simulations with the MPI-ESM, which are again very similar. The science question, if initial conditions in the hindcasts lead to more accurate retrospective predictions of sea-ice compared to the uninitialized simulations can be qualitative answered in this work. On considered timescales the simulated sea-ice extent and sea-ice concentration of uninitialized and initialized simulations provide the same results. However, further studies are required to finally answer this question.

As a next step, a verification system for example similar to the one proposed by Goddard et al. (2012) could be implemented in order to make quantitative declaration of the skill and the dependence on lead time. Reasons for the general underestimation of sea-ice cover in the Antarctic have to be examined in future studies. Also other parameters like the sea-ice thickness and volume should be investigated, since there is a significant shift from thick multiyear towards thinner first-year sea-ice.

6 Acknowledgements

This work was performed as part of the BMBF MiKlip Climate Model Validation by confronting globally Essential Climate Variables from models with observations (ClimVal project) and the DLR ESMVal (Earth System Model Validation) project.

At first I want to thank Veronika Eyring for giving me the opportunity to write this thesis and supervising me.

I also would like to thank Klaus-Dirk Gottschaldt for all his time he spent to support me with technical issues and Sabrina Wenzel and Matthia Righi, who helped me with NCL and Linux questions.

I enjoyed the time at the DLR Oberpfaffenhofen especially, because of the nice working atmosphere and would like to thank the “Abteilung 1” for that.

7 References

- Cavalieri, D. J., C. I. Parkinson, P. Gloersen, and H. J. Zwally. 1997. Arctic and Antarctic Sea Ice Concentrations from Multichannel Passive-microwave Satellite Data Sets: October 1978 to December 1996, User's Guide. NASA Technical Memorandum 104647. 17 pages.
- Cavalieri, D., Parkinson, C., 2008. Antarctic sea ice variability and trends, 1979–2006
- National Snow and Ice Data Center, University of Colorado, Boulder. All About Sea Ice: <http://nsidc.org/cryosphere/seaice/>
- Giorgetta, M.A. et al., 2013. Climate change from 1850 to 2100 in MPI-ESM simulations for the Coupled Model Intercomparison Project 5. JAMES, submitted 2013.
- Goddard, L., Kumar, A., Solomon, A., Smith, D., Boer, G., Gonzalez, P., Kharin, V., Merryfield, W., Deser, C., Mason, S.J., Kirtman, B.P., Msadek, R., Sutton, R., Hawkins, E., Fricker, T., Hegerl, G., Ferro, C.A.T., Stephenson, D.B., Meehl, G.A., Stockdale, T., Burgman, R., Greene, A.M., Kushnir, Y., Newman, M., Carton, J., Fukumori, I., Delworth, T., 2012. A verification framework for interannual-to-decadal predictions experiments. *Clim Dyn* (2013) 40:245-272, doi: 10.1007/s00382-012-1481-2.
- Hibler, W. D. III, 1979, A dynamic thermodynamic sea ice model. *J. Phys. Oceanogr.*, 9, 815-846
- Hübner, M., 2013. Evaluation of Sea-ice in the Max-Planck-Institute Earth System Model.
- Hunke, E.C., Dukowicz, J.K., 1997. An Elastic-Viscous-Plastic Model for Sea Ice Dynamics. *American Meteorological Society*. Volume 27.
- Ilyina, T., Six, K. D., Segsneider, J., Maier-Reimer, E., Li, H. and Nunez-Riboni, I., 2012 (submitted). The global ocean biogeochemistry model HAMOCC: Model architecture and performance as component of the MPI-Earth System Model in different CMIP5 experimental realizations.
- IPCC, 2007. Intergovernmental Panel on Climate Change (IPCC), *Climate Change 2007: The Physical Science Basis*. Contribution of Working Group I to the Fourth Assessment Report of the Intergovernmental Panel on Climate Change, Cambridge, United Kingdom and New York, NY, USA.
- Jungclaus, J. H., Keenlyside, N., Botzet, M., Haak, H., Luo, J.-J., Latif, M., Marotzke, J., Mikolajewicz, U., and Roeckner, E., 2006. Ocean circulation and tropical variability in the coupled model ECHAM5/MPI-OM. *Journal of Climate*, Vol. 19, 3952-3972.
- Jungclaus, J. H., Fischer, N., Haak, H., Lohmann, K., Marotzke, J., Matei, D., Mikolajewicz, U., Notz, D. and von Storch, J.-S., 2012 (submitted). Characteristics of the ocean simulations in MPIOM, the ocean component of the MPI Earth System Model.
- Marsland, S.J., Haak, H., Jungclaus, J.H., Latif, M., Röske, F., 2003. The Max-Planck-Institute global ocean/sea ice model with orthogonal curvilinear coordinates.
- Meehl, G.A.; Goddard, L., Murphy, J., Stouffer, R.J., Boer, G., Danabasoglu, G., Dixon, K., Giorgetta, M. A., Greene, A.M., Hawkins, E., Hegerl, G., Karoly, D., Keenlyside, N., Kimoto, M., Kirtman, B., Navarra, A., Pulwarty, R., Smith, D., Stammer, D., Stockdale, T., 2009. Decadal Prediction. Can it be skillful? *American Meteorological Society*, doi 10.1175/2009BAMS2778.1

Meehl, G.A., Goddard, L., Boer, G., Burgman, R., Branstator, G., Cassou, C., Corti, S., Danabasoglu, G., Doblas-Reyes, F., Hawkins, E., Karspeck, A., Kimoto, M., Kumar, A., Matei, D., Mignot, J., Msadek, R., Pohlmann, H., Rienecker, M., Rosati, T., Schneider, E., Smith, D., Sutton, R., Teng, H., van Oldenborgh, G.J., Vecchi, G., Stephen, Y., 2013. Decadal Climate Prediction: Un Update from the Trenches. American Meteorological Society, doi: 10.1175/BAMS-D-12-00241.1

Meinshausen, M., Smith, S.J., Calvin, K., Daniel, J.S., Kainuma, M.L.T., Lamarque, J.F., Matsumoto, K., Montzka, S.A., Raper, S.C.B., Riahi, K., Thomson, A., Velders, G.J.M. and van Vuuren, D.P.P., 2011. The RCP greenhouse gas concentrations and their extensions from 1765 to 2300. *Climatic Change*, 109(1-2): 213-241.

Müller, W.A., Baehr, J., Haak, H., Jungclaus, J.H., Kröger, J., Matei, D., Notz, D., Pohlmann, H., von Storch, J.S., Marotzke, J., 2012. Forecast skill of multi-year seasonal means in the decadal prediction system of the Max Planck Institute for Meteorology. *GEOPHYSICAL RESEARCH LETTERS*, VOL. 39, L22707, doi: 10.1029/2012GL053326, 2012.

Notz, D., F. A. Haumann, H. Haak, J. H. Jungclaus and J. Marotzke, 2013. Arctic sea-ice evolution as modeled by MPI-ESM, doi: 10.1002/jame.20016, *JAMES*, accepted.

Perovich, D. K., Polashenski, C., 2012. Albedo evolution of seasonal Arctic sea ice, *GEOPHYSICAL RESEARCH LETTERS*, VOL. 39, L08501, doi: 10.1029/2012GL051432, 2012

Pohlmann H., Jungclaus J., Köhl A., Stammer D., Marotzke J., 2009. Initializing Decadal Climate Prediction with the GECCO Oceanic Synthesis: Effects on the North Atlantic. DOI: 10.1175/2009JCLI2535.1

Rayner, N.A., Parker, D.E., Horton, E.B., Folland, C.K., Alexander, L.V., Rowell, D.P., Kent, E.C. and Kaplan, A., 2003. Global analyses of sea surface temperature, sea ice, and night marine air temperature since the late nineteenth century, *J. Geophys. Res.*, 108(D14): 4407

Reick, C., Raddatz, T., Brovkin, V. and Gayler, V., 2012 (submitted). The representation of natural and anthropogenic land cover change in MPI-ESM.

Richter-Menge J., Walsh J., Brigham L., Francis J., Holland M., Nghiem S., Raye R., Woodgate R., 2012. Seasonal to Decadal Predictions of Arctic Sea Ice, National Academy of Sciences: Challenges and Strategies, ISBN 978-0-309-26526-3

Semtner, A., 1976. A Model for the Thermodynamic Growth of Sea Ice in Numerical Investigation of Climate.

Smith, K.L., Polvani, L.M. and Marsh, D.R., 2012. Mitigation of 21st century Antarctic sea ice loss by stratospheric ozone recovery. *Geophysical Research Letters*, 39.

Solomon, A., Goddard, L., Kumar, A., Carton, J., Deser, C., Fukumori, I., Greene, A., Hegerl, G., Kirtman, B., Kushnir, Y., Newman, M., Smith, D., Vimont, D., Delworth, T., Meehl, G., Stockdale, T., 2010. Distinguishing the roles of natural and anthropogenically forced decadal climate variability. *Bulletin of the American Meteorological Society*, 92: 141-156.

Spreen, G., Kaleschke, L. and Heygster, G., 2008. Sea ice remote sensing using AMSR-E 89-GHz channels. *Journal of Geophysical Research-Oceans*, 113(C2).

Stevens, B., Giorgetta, M. A., Esch, M., Mauritsen, T., Crueger, T., Rast, S., Salzmann, M., Schmidt, H., Bader, J., Block, K., Brokopf, R., Fast, I., Kinne, S., Kornblueh, L., Lohmann, U., Pincus, R., Reichler, T.

and Roeckner, E, 2012. (submitted). The atmospheric component of the MPI-M Earth System Model: ECHAM6

Stroeve, J., Holland, M.M., Meier, W., Scambos, T. and Serreze, M., 2007. Arctic sea ice decline: Faster than forecast. *Geophys. Res. Lett.*, 34(9): L09501.

Stroeve, J.C., Kattsov, V., Barrett, A., Serreze, M., Pavlova, T., Holland, M. and Meier, W.N., 2012. Trends in Arctic sea ice extent from CMIP5, CMIP3 and observations. *Geophysical Research Letters*, 39.

Taylor, K.E., Balaji, V., Hankin, S., Juckes, M., Lawrence, B., 2010. CMIP5 and AR5 Data Reference Syntax (DRS): http://cmip-pcmdi.llnl.gov/cmip5/docs/cmip5_data_reference_syntax_v0-25_clean.pdf

Taylor, K.E., Stouffer, R.J. and Meehl, G.A., 2012. An Overview of Cmp5 and the Experiment Design. *Bulletin of the American Meteorological Society*, 93(4): 485-498.

Declaration of Authorship

I do solemnly declare that I have written the presented thesis by myself without undue help from a second person others and without using such tools other than that specified. Where I have used thoughts from external sources, directly or indirectly published or unpublished, this is always clearly attributed. Furthermore, I certify that this research thesis or any part of it has not been previously submitted for a degree or any other qualification at the Ludwig-Maximilians-Universität of Munich or any other institution in Germany or abroad.

Date

Signature